

Accepted Manuscript

Multi-analytical approach to the study of the European glass beads found in the tombs of Kulumbimbi (Mbanza Kongo, Angola)

Mafalda Costa, Pedro Barrulas, Luís Dias, Maria da Conceição Lopes, João Barreira, Bernard Clist, Karlis Karklins, Maria da Piedade de Jesus, Sónia da Silva Domingos, Peter Vandenabeele, José Mirão



PII: S0026-265X(19)30358-3
DOI: <https://doi.org/10.1016/j.microc.2019.103990>
Article Number: 103990
Reference: MICROC 103990
To appear in: *Microchemical Journal*
Received date: 14 February 2019
Revised date: 5 June 2019
Accepted date: 6 June 2019

Please cite this article as: M. Costa, P. Barrulas, L. Dias, et al., Multi-analytical approach to the study of the European glass beads found in the tombs of Kulumbimbi (Mbanza Kongo, Angola), *Microchemical Journal*, <https://doi.org/10.1016/j.microc.2019.103990>

This is a PDF file of an unedited manuscript that has been accepted for publication. As a service to our customers we are providing this early version of the manuscript. The manuscript will undergo copyediting, typesetting, and review of the resulting proof before it is published in its final form. Please note that during the production process errors may be discovered which could affect the content, and all legal disclaimers that apply to the journal pertain.

Multi-analytical approach to the study of the European glass beads found in the tombs of Kulumbimbi (Mbanza Kongo, Angola)

Mafalda Costa^{a,b}; Pedro Barrulas^b; Luís Dias^b; Maria da Conceição Lopes^{c,d}; João Barreira^c;
Bernard Clist^{e,f}; Karlis Karklins^g; Maria da Piedade de Jesus^h; Sónia da Silva Domingosⁱ;
Peter Vandenabeele^a; José Mirão^{b,j*}

^a Archaeometry Research Group, Department of Archaeology, Ghent University, Sint-Pietersnieuwstraat 35, B-9000 Ghent, Belgium. mafalda.costa@ugent.be; peter.vandenabeele@ugent.be

^b HERCULES Laboratory, University of Évora, Palácio do Vimioso, Largo Marquês de Marialva 8, 7000-554 Évora, Portugal. pbarrulas@uevora.pt; luisdias@uevora.pt; jmirao@uevora.pt

^c Research Center in Archaeology, Arts and Heritage Sciences, University of Coimbra, Palácio de Sub-Ripas, 3000-395 Coimbra, Portugal. conlopes@ci.uc.pt; joambarreira@gmail.com

^d Department of History, Archaeology and Arts, Faculty of Arts and Humanities, University of Coimbra, Largo da Porta Férrea, 3004-530 Coimbra, Portugal.

^e Department of Languages and Cultures, BantUGent – UGent Centre for Bantu Studies, Ghent University, Blandijnberg 2, 9000 Ghent, Belgium. bernardolivier.clist@ugent.be

^f Institut des Mondes Africains (IMAF), Paris, France

^g Society of Bead Researchers, Ottawa, Ontario, Canada. karlis4444@gmail.com

^h Instituto Nacional do Património Cultural (INPC), Rua Major Kanhangulo 77/79, 1267, Luanda, Angola. piedadejesus65@gmail.com

ⁱ Centro Nacional de Investigação Científica (CNIC), Avenida Ho Chi Min 201, 34, Maianga, Luanda, Angola. tasonia2000@yahoo.fr

^j Department of Geosciences, School of Science and Technology, University of Évora, Colégio Luís António Verney, R. Romão Ramalho 59, 7000-671 Évora, Portugal.

* Correspondence to:

José Mirão: jmirao@uevora.pt.

HERCULES Laboratory, University of Évora, Largo Marquês de Marialva 8, 7000-809 Évora, Portugal.

Phone number: +351 266 740 800

Abstract

The glass bead assemblages recovered during the 2014 excavations of the ruins of Kulumbimbi located in Mbanza Kongo (Angola) were analyzed by means of a multi-analytical minimally invasive methodology, which includes handheld X-ray fluorescence (hXRF), variable pressure scanning electron microscope coupled with energy dispersive X-ray spectrometry (VP-SEM-EDS), micro-Raman spectroscopy and laser ablation inductively coupled plasma mass spectrometry (LA-ICP-MS). Chemical data indicate that cobalt, copper, iron and manganese ions were used to produce the blue, green, reddish-brown and black hues, respectively. Lead arsenates, calcium phosphate, calcium antimonate, lead stannate, cassiterite and Pb-Sb-Sn oxide were used as opacifying agents. Chondrite-normalized trace element distribution and chondrite-normalized rare earth element patterns were used to determine the sand source used in the production of the different glass bead types. These distributions were also used to identify the manufacture location of the glass beads with previously unknown origin and production date. Based on the data collected, the glass beads from types 16, 20, 22, 24, 25, 46 and 47 have been assigned as Venetian.

Key-words: Mbanza Kongo; Kongo kingdom; glass beads; provenance; colorants and opacifiers; LA-ICP-MS

1. Introduction

The Kongo kingdom, an independent state from approximately the 14th to 19th century, was one of the largest constituted polities in sub-Saharan Africa, covering an area that extended from northern Angola to western Democratic Republic of the Congo [1–4]. The Portuguese navigator Diogo Cão first came into contact with the Kongo kingdom when he reached the mouth of the Congo river in 1483 [2]. Contact with the Portuguese had a huge impact in the Kongolesse society, and many Portuguese practices were readily adopted, especially religion and literacy [5]. Despite the fact that no written records exist prior to the arrival of the Portuguese, Thornton (2001) [1] estimated the founding date of the kingdom to ca. 1390, taking into consideration the oral tradition documented as Kings lists (*mvila*) and the accounts written by Europeans in the 16th and 17th centuries. This author has since attempted to reconstruct the history of the Kongo Kingdom further in time, making it follow the existence of the "Seven Kingdoms of Kongo dia Nlaza", a former polity that may have been fully incorporated into the kingdom by the 16th century [2].

Mbanza Kongo, the kingdom's capital, is located on a plateau, 600 m above the sea level in modern northern Angola. It is considered to be the oldest continuously occupied large settlement (or *Mbanza* in Kikongo) in West Central Africa if one excludes the brief thirty years of abandonment caused by the civil wars of the 17th and 18th centuries [6,7]. The Church of São Salvador (Figure 1a), currently known as Kulumbimbi, is a formerly Jesuit stone church built in 1548 and dedicated to Jesus the Savior [7]. The church was destroyed during the *Jaga*¹ invasions of the capital that took place during the reign of Kongo king Álvaro I (1568-1587 [7]), but was later rebuilt and elevated to the status of Cathedral in 1596 [8]. The current name Kulumbimbi, which originated in the oral traditions, means "what remained of the ancestors" in Kikongo [8]. Today the church ruins are one of a very short list of still standing architectural remains of the old kingdom's capital.

The recent addition (July 2017) of Mbanza Kongo to the UNESCO World Heritage List highlights the importance of the Kongo kingdom and of its capital in human history as a major interaction point between Africa and Europe from the late 15th century onwards.

This study focuses on a collection of over 3,000 glass beads recovered during the 2014 excavation campaign in the ruins of Kulumbimbi. European-manufactured glass beads were among the exotic goods brought to the Kongo kingdom via the oceanic trade routes most likely introduced by the Portuguese in the end of the 16th century. The glass beads, used as adornments or amulets, were a symbol of wealth, social status and political, cultural and religious affiliation [9,10]. Glass beads were also used as currency [10,11]. The study of European trade beads can, therefore, shed light on economic interactions and consumption patterns on a chronological level [9].

The presence of European beads in the capital of the Kongo kingdom is convincing evidence of the existence of a transatlantic triangular trading system, in place between the 16th and 19th

¹ "A generic Kikongo term applied to rootless people who often lived by raiding" [1].

century, that allowed the presence of European manufactured products in Africa, the trade of African slaves to America and of raw materials from America and Africa to Europe. Therefore, this work must contribute knowledge of the commerce between Europe and western central Africa, by:

- Identifying the European production regions of these manufactured products;
- Recognizing the technology and the materials used in the beads production.

Although glass usage and technology has changed throughout time, glass is typically made of four main components: 1) glass formers or vitrifiers, 2) glass modifiers or fluxing agents, 3) glass stabilizers, 4) opacifiers and glass coloring and/or decoloring agents. Silica, either in the form of sand, or coarse quartz pebbles is the most common glass former. The fluxing agent, usually an alkaline oxide (*e.g.* an evaporitic deposit raw material), was used to lower the melting temperature, while glass stabilizers, such as lime, were added to make the mixture more stable and resistant to deterioration [12,13].

The use of distinct glass recipes and different raw material sources causes glass composition to change according to its provenance. The development of minimally invasive analytical techniques capable of accurately and precisely determining trace element concentrations, such as LA-ICP-MS, greatly contributed to ancient glass studies. In fact, chemical characterization of glass artefacts, with a high emphasis on trace element analysis, particularly rare earth element (REE) concentrations, has been successfully carried out to determine the nature and provenance of the raw materials used in their manufacture and to attribute their production to a specific workshop or region (*e.g.* [14–26]). De Raedt et al. (2001) [15], for instance, has successfully used European shale normalized-REE patterns to distinguish between Venetian glass vessels and *façon-de-Venise* vessels made in Antwerp, while Saitowitz (1996) [14] used chondrite-normalized REE patterns to confirm the existence of trade networks between southern Africa, Egypt and the Islamic mercantile network in ca. 900-1200 A.D.

Despite the fact that European trade beads were vital in the economic and societal interactions throughout Africa, most analytical studies focus on assemblages found in North America [27–33]. The chemical characterization of European trade beads found in African contexts is rare [16,34–37], as most works focus on glass beads from the Islamic mercantile network or the Indian Ocean trade [14,18,19,21,22,34,35,38–41].

To determine the composition of European glass beads from Kulumbimbi, a multi-analytical minimally invasive methodology was applied, which includes handheld X-ray fluorescence (hXRF), variable pressure scanning electron microscope coupled with energy dispersive X-ray spectrometry (VP-SEM-EDS), micro-Raman spectroscopy and laser ablation inductively coupled plasma mass spectrometry (LA-ICP-MS). The results were interpreted considering the probable provenance, raw materials used and technology available in the production of these artefacts. Special effort was made to understand the processes of glass coloring and opacification.

2. Materials and Methods

2.1. Materials

Three thousand three hundred and sixty-seven glass beads were recovered from four tombs during the 2014 excavation campaign carried out in the ruins of Kulumbimbi (Mbanza Kongo, Angola) by M. Conceição Lopes (University of Coimbra, Portugal), and Christophe Mbida and Raymond Assombang (University of Yaoundé I, Cameroon). The morphological characteristics of each glass bead, including color, size and manufacturing technique were assessed by the archaeological team. These characteristics allowed the glass beads to be subdivided into typological groups. A detailed list of each typological group including untested possible origin and date can be found in Table S1 (Supplementary information). This burial, which contained the remains of a 22-year-old woman (Figure 1b), had both glass beads (2903) and *Pusula depauperata* shell beads (67), while the remaining three tombs (burials 2-4) contained only glass beads.

Three hundred glass beads (ca. 10% of the total number of specimens recovered) were analyzed *in situ* by handheld x-ray fluorescence (hXRF). A smaller selection of 30 glass beads was then selected to be transported to Europe for laboratory analyses.

2.2. Handheld X-ray fluorescence (h-XRF)

A handheld XRF Bruker™ Tracer III SD® with a silicon-drift (SDD) detector (XFlash®) and a Rh-target delivering a polychromatic X-ray beam of 3 x 3 mm was used for *in-situ* XRF analysis. Spectra were recorded using a voltage of 40 kV; a current intensity of 35 µA was applied, as well as vacuum conditions, during a 120-second real-time count. All spectra were recorded using the S1PXRF software (Bruker™) and processed using the Artax (Bruker™) software in order to obtain semi-quantitative data.

Each sample was analyzed in one or more locations according to their size and to their color – mono-colored or multi-colored. The generated net areas of the fluorescence lines were normalized to the counts of the Rh K α lines [42].

2.3. Variable pressure scanning electron microscope coupled with energy dispersive X-ray spectrometry (VP-SEM-EDS)

VP-SEM-EDS analyses were carried out using a Hitachi™ S3700N SEM coupled to a Bruker™ XFlash 5010 SDD EDS Detector® with an energy resolution of 124eV in the MnK α line. The samples were analyzed at low vacuum (40 Pa) and with an accelerating voltage of 20 kV. The variable pressure approach allows imaging and chemical analysis without the need of coating. The compositional data was acquired using the Esprit1.9 software and a standardless quantification. The SEM images were acquired in the backscattering mode.

2.4. Micro-Raman Spectroscopy

Raman spectra were recorded using a Bruker™ Optics SENTERRA dispersive Raman spectrometer coupled with a BX51 Olympus™ microscope. The instrument is equipped with a green Nd:YAG laser (532 nm) and a red diode laser (785 nm). At least three spectra per sample were acquired, using both lasers, at high resolution (3–5 cm^{-1}) and in the range of 60–2750 cm^{-1} and 80–2642 cm^{-1} for the 532 nm and 785 nm lasers, respectively. The system uses a thermo-electrically cooled CCD detector, operating at -65 °C. The power of each laser and the instrument itself is controlled by the Bruker™ OPUS software. The measuring time, laser power, and number of accumulations were set to obtain a good signal-to-noise ratio. The 20× objective was used for all the samples, with a spot size of approximately 10 μm .

The collected Raman spectra were further processed in GRAMS (ThermoFisher Scientific™). In order to characterize the glass matrix, a 4-segment liner baseline was subtracted using fixed points at approximately 200, 700, 800 and 1200 cm^{-1} [34,36,43–46]. The glass massifs were subsequently subjected to curve fitting in order to allow for reproducible results and for comparison with published data.

2.5. Laser ablation inductively coupled plasma mass spectrometry (LA-ICP-MS)

LA-ICP-MS analyses were conducted using a CETAC LSX-213 G^{2+} laser ablation system coupled to an Agilent™ 8800 Triple Quad ICP-MS. The glass beads were mounted on the ablation cell without any previous sample preparation. A 100 μm spot size with a frequency of 20 Hz and a laser output energy of 80 % (3 mJ/pulse at 100%) was used to analyze 8-12 spots in each multi-colored glass beads, four in each glass color, while the mono-colored glass beads were analyzed in 4 different locations. Each spot had a total acquisition time of 60 s, including a 10 s washout. Helium, with a flow of 1 L/min, was used as a carrier gas in the LA system and the ICP-MS data was acquired in MS/MS mode. The NIST 612 glass standard was used for the calibration of the ICP-MS prior the analysis. Fractionation was monitored using the $^{238}\text{U}/^{232}\text{Th}$ ratio, while oxide formation was measured using the $^{248}\text{ThO}/^{232}\text{Th}$ ratio. Equipment sensibility was also examined. The NIST 612 glass standard was analyzed at the beginning and end of each sequence and at 6-10 spot intervals for drift determination and correction if needed. The isotopes that were analyzed and their respective dwell times can be found in Table 1. Data of two different Ca, Fe and Zn isotopes were acquired and used to determine possible instrumental interferences. Elemental concentrations were determined using off-line calculations and data reduction with the GLITTER® software, using NIST 612 as primary reference material (recommended concentrations reported by [47]) and SiO_2 as an internal standard for the samples and reference

material. The first 4 or 5 seconds of ablation were discarded to eliminate the interference of surface contamination and weathering.

Table 1: Isotopes analyzed by LA-ICP-MS and their respective dwell times.

Dwell time (ms)	Isotope
5	^{23}Na ; ^{27}Al ; ^{28}Si ; ^{39}K ; ^{44}Ca ; ^{55}Mn ; ^{56}Fe
10	^{11}B ; ^{24}Mg ; ^{43}Ca ; ^{47}Ti ; ^{52}Cr ; ^{55}Mn ; ^{57}Fe ; ^{59}Co ; ^{60}Ni ; ^{63}Cu ; ^{66}Zn ; ^{67}Zn ; ^{75}As ; ^{85}Rb ; ^{88}Sr ; ^{89}Y ; ^{90}Zr ; ^{118}Sn ; ^{121}Sb ; ^{208}Pb
20	^{31}P ; ^{45}Sc ; ^{51}V ; ^{93}Nb ; ^{133}Cs ; ^{137}Ba ; ^{139}La ; ^{140}Ce ; ^{141}Pr ; ^{146}Nd ; ^{147}Sm ; ^{153}Eu ; ^{157}Gd ; ^{159}Tb ; ^{163}Dy ; ^{165}Ho ; ^{166}Er ; ^{169}Tm ; ^{172}Yb ; ^{175}Lu ; ^{178}Hf ; ^{181}Ta ; ^{209}Bi ; ^{232}Th ; ^{238}U

3. Results and Discussion

Due to the high number of samples and analytical techniques employed in this study, this section has been subdivided according to the methodology used. The importance of each analytical technique has been highlighted, as well as their unique shortcomings.

3.1. Handheld X-ray fluorescence (hXRF) and variable pressure scanning electron microscope coupled with energy dispersive X-ray spectrometry (VP-SEM-EDS)

The handheld XRF measurements were performed in Mbanza Kongo, northern Angola. This technique has proven to be a fairly inexpensive, fast and efficient technique to use when dealing with a large number of samples [48–50] in difficult analytical conditions. This non-destructive technique is therefore commonly employed in the study of large assemblages in order to screen and group materials for further sub-sampling and analysis using other techniques [48,50]. Since the Bruker™ Tracer III-SD is limited to the detection of elements with $Z > 11$, a clear distinction between glass types, generally based on the type of fluxing agent used in their manufacture, is not possible using this technique. Nonetheless, the use of bulk composition to produce elemental bi-plots allows a better understanding of the data collected and can be used, as a first approach, to determine differences between glass beads from the same typology, and affinities between chemical elements or different glass beads typologies.

Complementary, VP-SEM-EDS was used to perform a microstructural and micro-analytical characterization, to initially classify the beads according to glass type – soda-rich, potash-rich or mixed alkali glass – and to access the lead content. Point analysis and elemental mapping was also used to identify the chemical composition of the inclusions present in the glass beads. It is important to note that SEM-EDS is a surface-sensitive technique, having an analysis depth of approximately 1-2 μm [51], whereas hXRF has an analysis depth of a few microns to a few

millimeters depending on the material's absorption coefficient [52–54]. Moreover, as both systems use an X-ray energy dispersive spectrometer to obtain the chemical composition of the beads, the data are complementary.

3.1.1. Blue glass beads (types 1, 8, 12, 13, 22 and 24)

The VP-SEM-EDS analysis revealed that the glass beads from types 1, 8, 12 and 13 are composed of potash-rich glass while the glass beads from type 22 and 24 consist of mixed alkali glass (Table S2 – Supplementary information).

Significant amounts of Co were detected by hXRF in the blue beads from types 8, 12, 13, 22 and 24 (Figure 2a). Relatively smaller amounts of cobalt are also present in the pale blue beads classified as type 1 (Figure 2a). Co(II) ions are among the most common coloring agents present in ancient glass [55]. The presence of this transition metal ion in a tetrahedral coordination [56,57] imparts a dark blue hue to the glass [27,29,32,37,55,57–61]. Moreover, even when present in small concentrations, due to their high absorption coefficient, cobalt ions produce a distinct blue color [32,55,61]. It is important to note that the glass beads classified as type 24 are enriched simultaneously in cobalt and copper, causing them to have a lighter blue hue (Figure 2a). While the addition of Cu could have been unintentional, this transition element's divalent ion, in an octahedral coordination [56], is known to impart a turquoise color to glass [37,57,62]. Cobalt, although relatively common in nature, is generally exploited as a by-product of the extraction of nickel, silver, gold, lead and zinc [63]. Cobalt can also be exploited from arsenic-rich and Fe-rich minerals [63]. Many studies have attempted to uncover the provenance of the cobalt blue pigments based on the association between Co and other minor and trace elements [29,58,60,64–67]. However, the use of different techniques with different detection limits has made it very difficult to establish a true chronology of cobalt use, and, unfortunately, many pigment sources remain unknown [66].

A careful examination of the hXRF results revealed that cobalt was associated with: a) Ni and As in types 12 and 13; b) Ni, Zn and Pb, in type 1; c) Cu, Ni, Zn, Fe and Cr in type 24; and d) Ni, As, Zn, Fe, and Bi in types 8 and 22 (Figure S1 – Supplementary information). According to Dayton (1981) [68] and Gratuze et al. (1992) [64], the parageneses of Co-Ni-As minerals can be found in the Schneeberg mines (Erzgebirge, Germany). The cobalt-bearing minerals extracted from this region are thought to have been used between the end of the 15th and the 18th centuries A.D. [29,65,67]. The glass beads from types 12 and 13 have been associated to the Bohemian glass production of the 19th century. While an earlier manufacture date cannot be excluded [31], it is important to note that Gratuze & Janssens (2004) [60] mention a cobalt ore of unknown provenance used in the 19th century having a chemical association of Co-Ni-As.

The chemical association of Co-Zn-Pb has been linked to the Freiberg district (Saxony, Germany) [64,65,67]. Although Co-Ni veins are less abundant in this district, they are nonetheless present [69]. The polymetallic veins present in the Freiburg region are a known source of cobalt pigments used between the 13th and 15th centuries A.D. [65,67]. The type 1 pale blue glass beads display the Co-Ni-Zn-Pb chemical association; however, since the glass beads are thought to have been produced at a later date, between 1680 and 1890, it is possible that a different pigment source was used.

Finally, to our knowledge, the chemical association Co-Ni-As-Zn-Fe-Bi found in the glass beads from types 8 and 22, and the association between cobalt and Cu, Ni, Zn, Fe, Cr and As found in the type 24 glass beads have not been mentioned in any other glass studies.

The amount of As present in the type 8 glass beads (Figure 2b), detected by both hXRF and VP-SEM-EDS (Table S2 – Supplementary information), cannot be explained exclusively by the Co pigment. The chronology of opacifiers developed by Hancock et al. (1997) [28] could suggest that these glass beads were produced between the very late 18th century and the early 20th century. However, Hancock et al. (1997) [28] used neutron activation analysis to determine the composition of the glass beads in their study, and these authors later suggested that the glass beads studied were, in fact, leaded [33]. Kenyon et al. (1995) [27] mentions that As could be used to remove air bubbles from the glassy melt in order to produce a clearer, more transparent glass. However, since these glass beads are opaque and there is an obvious enrichment and association between Ca and P, suggesting that calcium phosphates were used as opacifying agents, the use of As as a fining agent seems implausible. Arsenic is also a known decolorant [70]. While the exact purpose of the introduction of As remains unknown, calcium phosphate, generally introduced in the form of burnt bones, has been used as an opacifier since the 5th century AD and is commonly mentioned in Venetian recipe books since the 14th century [13,71]. Calcium phosphates were also most likely used to opacify the glass beads from type 1 and 13 since the VP-SEM-EDS analysis revealed an enrichment in both Ca and P in these glass beads (Table S2 – Supplementary information).

The type 8 glass beads also have minor amounts of barium detected by hXRF (Figure S1 – Supplementary information). Barium occurs in large deposits throughout the world mostly as barium sulfate (barite; [72]). In fact, barite has been found as a heavy mineral in glass-making sand [73]. However, barium has also been known to substitute calcium in carbonates [74] and even in apatite (calcium phosphate) without any significant changes in the crystalline structure [75]. The lack of correlation between Ca and Ba suggests that the latter is the result of the use of impure sands rich in barite.

The hXRF Sb-Ca plot (Figure 2c), on the other hand, revealed that calcium antimonates were used as opacifying agents in the manufacture of the type 22 blue beads. Calcium antimonates have been used in glass production since the 15th century B.C. [13,71,76]. Opacifying agents could not be detected in the blue glass beads from types 12 and 24 because they are transparent.

3.1.2. Red and red-on-white glass beads (type 2, 3 or 4, 6, 7, 9, 10, 11, 14, 15 and 19)

Red glass can be produced by the addition of metallic gold [13,31,56,77] or metallic copper (nano-) particles [13,30,55,56,77–79]. The metallic copper particles disperse the light, rendering the glass opaque [78]. Many authors have shown that cuprous oxide (Cu_2O) can also be used to impart a ruby color to the glass, commonly referred to as “sealing wax red” [13,16,30,61,77,79,80]. Finally, since the development of cadmium red pigments in 1892 [81–83], these pigments have been used to produce both red glass [13,84] and red glass beads [37,83]. An initial assessment of the hXRF data of the red and red-on-white glass beads revealed detectable amounts of copper, accompanied by significant amounts of lead. The enrichment in lead is very significant (commonly reaching 40-50 wt.% according to VP-SEM-EDS data; Table S2 – Supplementary information) indicating that this element is acting as a glass former. The production of red glass by dispersing cuprite crystals in a lead-rich glass matrix has been reported by Licenziati & Calligaro (2016) [61]. However, it is important to note that no red-coloring elements were detected in any of the red or red-on-white glass beads by VP-SEM-EDS. Therefore, the use of other colorants such as trace amounts of metallic gold, as reported by Burgess & Dussubieux (2007) [31], cannot be excluded.

Lead is particularly important in glass production since it can assume different roles; it can act as a glass former and modifier, but it can also interact with other elements present in the glass melt, causing the precipitation of crystals that influence both color and transparency [13]. VP-SEM-EDS analysis showed that all red and red-on-white beads were enriched in both lead and arsenic (Table S2 – Supplementary information). In fact, the hXRF Pb-As plot (Figure 2c) revealed a clear association between these two elements, which suggests that lead arsenates were used as the main opacifying agents. Lead arsenates were developed by the Venetian glass industry in the late 16th century [34,35,85,86], but were only broadly used since the 19th century [34,35].

The hXRF Pb-Sn plot (Figure 2d), on the other hand, shows that lead arsenates were not the only opacifiers used in the manufacture of the red and red-on-white glass beads. In fact, these beads are also enriched in tin, which could indicate the combined use of cassiterite (SnO_2) and lead arsenates. The presence of both tin oxide and lead arsenates has been reported in 19th century enamels [46,87]. Lead arsenates were introduced in the Limoges production in the 18th century, gradually substituting cassiterite, although the combined use of these opacifiers has been found in many 19th century artefacts [46,87]. The first use of cassiterite in glass production can be traced to the 4th century A.D. [71,76].

Several of the red-on-white glass beads were broken in half, which allowed the acquisition of elemental data from their white core by VP-SEM-EDS. All white glass present in the red and red-on-white glass beads was found to be lead-rich (Pb ~ 50-65 wt.%; Table S2 – Supplementary information). The presence of lead arsenates can account for the glass’ white hue.

3.1.3. Black glass (types 16, 20 and 23)

The VP-SEM-EDS analysis revealed that the glass beads from types 16, 20 and 23 are composed of soda-rich glass (Table S2 – Supplementary information).

The hXRF results of the black beads classified as types 16, 20 and 23 revealed significant amounts of Mn and Fe in their composition (Figure 2e). The enrichment in both manganese and iron was further confirmed by VP-SEM-EDS (Table S2 – Supplementary information). Combining metallic ions such as iron and manganese has been used to produce black hues [37,88].

Elements associated to opacifying agents were not detected in these glass beads by hXRF (Figures 2b, 2c and 2d) or VP-SEM-EDS (Table S2 – Supplementary information).

3.1.4. Green glass beads (type 46)

The green glass beads from type 46 are composed of lead-rich glass as shown by both the hXRF (Figures 2b and d) and VP-SEM-EDS data (ca. 49 wt.%; Table S2 – Supplementary information). Significant amounts of copper and iron were also detected by these two analytical techniques (Figure 2f and Table S2 – Supplementary information). According to Burgess & Dussubieux (2007) [31], although copper ions in their divalent state are generally used to produce turquoise glass, when they are dispersed in a lead-containing glass, the resulting hue is green. La Delfa et al. (2008) [89] determined that the amount of lead greatly influences the final green hue of a glass, when maintaining a stable Cu concentration. Iron, on the other hand, can be used to produce a wide range of colored glass, from yellow and amber/brown colors to green [37,55,57,59,62]. Since the ferric ion can be a blue chromophore and the ferrous ions can impart a yellow color, the final hue will be linked to the Fe(II)/Fe(III) ratio present in the glass [37,55,62]. In this case, iron was most likely introduced unwillingly, as an impurity in the copper or sand source, although its use to obtain a specific green hue cannot be excluded.

The hXRF Pb-Sn plot (Figure 2d) shows that there is an association between these two elements in the green type 46 glass beads, suggesting the use of lead stannate. Lead stannate or lead-tin yellow, was introduced as a colorant and opacifier in the 4th century A.D. [26,71,76] and was used to produce yellow opaque glass or to produce yellow-green hues when mixed with blue colorants [39,55,86,90].

3.1.5. Green glass beads with white and brownish-red stripes (type 5)

The multi-colored beads classified as type 5 are thought to be of Venetian origin, although their manufacture date is unknown. These beads are mostly composed of green glass but have three sets of reddish-brown stripes flanked by two white stripes.

The VP-SEM-EDS analysis revealed that the green body and the reddish-brown stripes consist of mixed alkali glass, with significant amounts of lead (12-30 wt.%), while the white stripes are

composed of lead-rich glass (61 wt.% Pb) (Table S2 – Supplementary information). Arsenic was also detected in both the green and white glass, which due to the aforementioned presence of lead, suggests the use of lead arsenates as the main opacifiers. In fact, the hXRF Pb-As plot (Figure 2b) shows a clear association between these two elements in the type 5 glass beads. The presence of lead arsenates in the type 5 glass beads indicates a manufacture date after the late 16th century [34,35,85,86].

A careful examination of the hXRF (Figure 2b, 2c and 2d) results also revealed an association between lead, antimony and tin, suggesting the use of a ternary Pb-Sb-Sn oxide. Lead antimonates have been used alongside calcium antimonates since the 15th century B.C. [13,71,76]. The first has also been used as a colorant, imparting a characteristic opaque yellow color to the glass [13,71,91]. Tin-based opacifiers, are thought to have been introduced by the Roman glass-making industry in the 4th century A.D., gradually substituting antimony-based opacifiers [26,71,76]. However, recent studies have shown that the pyrochlore structure of lead antimonates, commonly referred to as $Pb_2Sb_2O_7$, allows other elements, such as tin, to substitute antimony [91–95]. These pyrochlores or ternary Pb-Sb-Sn oxides, have been found in yellow Roman glass, being responsible for both their color and their opacification [26,91,93,96,97], and are thought to have been artificially produced and added to the molten glass [26,91,97]. This is consistent with the production of the Muranese yellow opacifier *anime* (or *anima*); 18th and 19th century Venetian glassmaking treaties describe how a synthesized lead-tin yellow pigment was mixed with antimony sulfide, minium (Pb_3O_4) and sand to obtain this yellow pigment which was later added to the glass [86,91,93,97]. Ternary Pb-Sb-Sn oxides have also been found in late 15th-early 16th century enameled Venetian glass objects [90], 17th century paintings [98], 18th century tesserae [95] and 18th century Nevers lampworking glasses [91,93].

Significant amounts of copper, together with minor amounts of iron were detected in the green glass. As previously mentioned, Cu(II) imparts a turquoise color to glass, while iron can be added to produce specific hues depending on the Fe(II)/Fe(III) ratio [37,57,62]. The presence of the yellow ternary Pb-Sb-Sn opacifier, suggests that the final green hue was obtained by combining the copper and iron blue colorants with the yellow opacifier as suggested by other authors [61,86,90,91,99,100].

The reddish-brown stripes were found to be enriched in iron, which has been known to produce similar reddish hues [37,59]. The white glass' color can be explained by the presence of lead arsenates.

3.1.6. White glass beads (types 25 and 47)

The VP-SEM-EDS analysis revealed that the white beads classified as types 25 and 47 are composed of mixed alkali glass (Table S2 – Supplementary information). The glass beads from type 25 were found to be extremely porous. Most likely due to the burial conditions, aluminosilicates now fill these pores, giving the glass beads a more yellowish hue. The hXRF Sb-Ca plot (Figure 2c), revealed an association between these two elements, suggesting that calcium

antimonates were used as opacifying agents in the manufacture of the type 25 white beads. In fact, VP-SEM-EDS analysis showed that calcium antimonate crystals were abundantly dispersed throughout the glass matrix (Figure 3). As previously mentioned, calcium antimonates have been used in glassmaking since the 15th century B.C. [13,71,76].

Antimony and calcium were also found to be associated in the type 47 glass beads. Calcium antimonate aggregates were also found in these beads by VP-SEM-EDS.

3.1.7. White glass beads with blue and pink stripes (Type 17)

The multi-colored beads classified as type 17 are thought to be of Venetian origin and manufactured between the 18th and 19th century. These beads are white with two navy and two pink stripes. VP-SEM-EDS analysis revealed that navy and pink stripes consist of mixed alkali glass, with significant amounts of lead (ca. 32-37 wt.%), while the white glass is lead-rich (Pb > 55 wt.%) (Table S2 – Supplementary information). Arsenic was also detected in all the glass colors, which due to the aforementioned presence of lead, suggests the use of lead arsenates as the main opacifiers. In fact, the hXRF Pb-As plot (Figure 2b) shows a clear association between these two elements in the type 17 glass beads. It is also worth noting that the glass beads from types 15 and 17, although contemporary, have different As contents, suggesting the use of different recipes in their manufacture.

No colorants were identified by VP-SEM-EDS in the blue and pink stripes. However, blue stripes have the distinctive navy-blue hue characteristic of Co(II)-colored glass, and it is possible that the pink hue was produced by adding minor amounts of copper or gold to produce a red hue that became pinkish when combined with the initial white glass.

Handheld XRF analysis also revealed an association between lead and tin, suggesting the use of lead stannate or lead-tin yellow as a second opacifier. Lead stannate imparts a yellow color to the glass, but as it is combined with the white lead arsenates, can account for the creamy white hue of the type 17 glass beads. It can also be responsible for the lighter blue hue of the blue stripes and the slight orange undertone of the pink stripes.

3.2. Micro-Raman Spectroscopy

Silicate glass, the most common type of archaeological glass, can be described as a disordered 3D network of SiO₄ tetrahedra, where the oxygen ions act as bridges between the different tetrahedral [36,44,45,101,102]. The Raman spectrum of a glass can, thus, be seen as the signature of the silicate network, with two large massifs, corresponding to the bending and stretching modes of the Si-O bonds, centered at approximately 500 cm⁻¹ and 1000 cm⁻¹, respectively [36,44,45,101,102]. The introduction of glass modifiers induces the breakdown of the siloxane

bands, creating non-bridging oxygens (NBOs). The arrangements of the SiO_4 tetrahedra can be described according to the number of NBOs from Q_0 (isolated tetrahedral with 4 NBOs) to Q_4 (pure SiO_2 with zero NBOs). The degree of polymerization of the network decreases with the increase of the amount of modifiers, and, therefore, the amount of NBOs [45]. The degree of polymerization or polymerization index (I_p) can be calculated as the ratio between the bending and stretching areas ($I_p = A_{500}/A_{1000}$) [34,36,40,44,45,101,102]. Colomban (2003) [101] developed an empirical relationship between the I_p and the firing temperature of glass. Micro-Raman spectroscopy due to its confocality and micrometric spatial resolution, also allows the identification of inorganic compounds dispersed in the glassy matrix and responsible for its color and opacity [34–37,45,46,57,61,71,85,94,101–104].

The calculated I_p and their respective firing temperature can be found in Table 2. It is important to note that the polymerization index has not been calculated when inorganic phases were found to be superimposed on the glass Raman signature. The inorganic phases acting as colorants and/or opacifiers, as well as the remains of the raw materials used in the production of poor melting quality glass, identified by micro-Raman spectroscopy can be found in Table 3.

Table 2: Polymerization index and corresponding firing temperature after Colomban (2003) [101]. The polymerization index was not calculated when inorganic phases were found to be superimposed on the glass Raman signature.

Glass bead type	Color	Polymerization index (I_p)	Estimated firing temperature ($^{\circ}\text{C}$)
5	Green	0.60	800
	White	-	-
	Reddish-brown	-	-
12	Blue	0.93	1000
20	Black	0.71	800-1000
22	Pale blue	0.92	1000
23	Black	0.75	800-1000
24	Blue	0.97	1000

Table 3: Inorganic phases (coloring agents, opacifiers and other crystalline phases) identified by micro-Raman spectroscopy. Characteristic band positions are indicated.

Inorganic phase	Raman signature	Glass bead type (glass color)	References
Anglesite (PbSO_4)	978-979 cm^{-1}	1 (pale blue), 12 (blue), 13 (blue)	[105–109]
Bindhemite ($\text{Pb}_2\text{Sb}_2\text{O}_7$)	138, 334, 511 cm^{-1}	3 or 4 (crème)	[61,85,103,104]
Calcium antimonate ($\text{Ca}_2\text{Sb}_2\text{O}_7$)	481, 634 cm^{-1} 483, 634 cm^{-1}	25 (white) 47 (white)	[34–37,57,61,85,94,104]
Calcium phosphate (PO_4^{3-})	959 cm^{-1}	1 (pale blue), 7 (white), 8 (blue), 13 (blue)	[34–37,71,102,108–111]

vibrations)			
Cassiterite (SnO ₂)	477, 637, 782 cm ⁻¹ 479, 638, 783 cm ⁻¹ 634-637 cm ⁻¹	3 or 4 (white) 7 (white) 17 (white)	[36,37,45,46,61,104,112]
Quartz (SiO ₂)	465 cm ⁻¹	16 (black)	[37,85,101,108,109]
Lead arsenates	814-831 cm ⁻¹	2 (red), 3 or 4 (red), 5 (white), 5 (reddish-brown), 6 (white), 6 (red), 7 (white), 7 (red), 9 (white), 9 (red), 10 (white), 10 (red), 11 (white), 11 (red), 14 (red), 15 (red), 17 (white), 17 (pink), 17 (blue), 19 (white), 19 (red)	[34–36,46,85,113–116]
Microcline (KAlSi ₃ O ₈)	475, 513 cm ⁻¹	46 (green)	[109]
Orthoclase (KAlSi ₃ O ₈)	478 cm ⁻¹	16 (black)	[109]
Rutile (TiO ₂)	444 cm ⁻¹	16 (black)	[85,108,109]
Unidentified sulfate phases (SO ₄ ²⁻ vibrations)	618, 981, 1141 cm ⁻¹ 981-982 cm ⁻¹	8 (blue) 2 (red), 3-4 (red), 7 (red), 9 (white), 9 (red), 10 (red), 11 (red), 12 (blue), 15 (red)	[36,109,117]
Titanium dioxide (TiO ₂)	140-150 cm ⁻¹	1 (pale blue), 5 (white), 9 (red), 9 (white), 12 (blue), 13 (blue), 16 (black), 17 (pink), 17 (blue), 47 (white), 20 (black, 22 (pale blue), 23 (black), 24 (blue), 25 (white)	[37,108,118–122]
Titanium dioxide (TiO ₂) or Litharge (PbO)	147 cm ⁻¹	2 (red), 3 or 4 (white), 6 (white), 7 (red), 10 (red), 17 (white), 19 (red)	[37,107,123,124]
α-Wollastonite (CaSiO ₃)	985 cm ⁻¹	7 (white), 14 (red)	[102]

3.3. Laser ablation inductively coupled plasma mass spectrometry (LA-ICP-MS)

Following the VP-SEM-EDS and micro-Raman spectroscopy analysis, a sub-sampling was performed in order to diminish the total number of samples. The possible origin and date of manufacture, as well as the number of samples available per type was taken into account. When a large number of samples from the same glass bead type was available, two specimens (*a* and *b*) were chosen to test for homogeneity and consistency between visually identical glass beads.

3.3.1. Chemical glass types

The ternary diagram of the normalized concentrations of Na_2O , $\text{MgO} + \text{K}_2\text{O}$ and CaO has been used to define the main chemical glass types based on their alkali metal source [60,125,126]. Figure 4 shows that all the glass beads in this study fall into one of the following chemical glass types: the soda-lime plant ash glass (II), the mixed alkali soda-potash glass (III) or the potash-lime plant ash glass (IV) [60].

The Venetian red and red-on-white glass beads from types 2, 3 or 4, 7, 10, 14 and 15, as well as the pink stripe from type 17, were found to be composed of mixed soda-potash glass (group III), while the remaining Venetian glass beads, type 5 and 17, fall either within the soda-lime plant ash compositional window (group II) or in between the two compositional groups. It is important to note that the type 17 glass beads appear to have been produced using two distinct recipes since the white and blue stripes fall under the compositional window of plant ash soda-lime glass (group II), while the pink stripes have a mixed soda-potash composition (group III). The Venetian glass making industry traditionally used soda plant ash as their main glass modifier [13,97,127]. These halophytic plant ashes, known as *allume catina*, were imported from the Levantine coast since the 13th century [13,127] and are commonly mentioned in treaties from the 16th and 17th centuries [13]. Lower quality soda plant ash (*barilla*) imported from Spain or produced by burning local plants was used from the 17th century onwards [13]. However, potash plant ashes, produced by burning inland plants, were occasionally used since the 15th century [13]. Recipes from the 16th and 17th centuries also mention tartar from wine barrels (*gripola di vino*) as a possible potash source [13]. The uncharacteristically high K concentrations found in all the Venetian glass beads can be explained by the use of low quality plant ash [31], or by the combined use of *allume catina* and *gripola di vino* as mentioned in the 1536 anonymous manuscript of Montpellier [13].

The glass beads from types 1, 8, 12 and 13, on the other hand, are composed of potash-lime plant ash glass (group IV). Potash-lime crystal glass was developed in Bohemia in 1676 by Johan Kunckel and increasingly gained popularity as an alternative to the Venetian *cristallo* glass [97]. However, the development of the first potash-lime glasses can be traced to the northern and central European production centers [127]. These glasshouses were founded during the Roman empire and were located in heavily forested areas to allow easy access to furnace fuel [127]. After the fall of the Roman empire, the knowledge of glass making was not lost, but since the import of mineral soda (natron, the main fluxing agent used in the production of Roman glass) ceased, glass makers started to use wood ash as the primary glass for glass production around 800 A.D. [127]. This glass, produced throughout the Middle Ages, is known as forest glass (or *Waldglas*). It is therefore likely, that the type 8 blue glass beads were produced in Central Europe, although the exact location of their manufacture remains unknown.

The glass beads of unknown origin and date, types 16, 20, 23, 25 and 47 and types 22, 24 and 46, fall within the soda-lime glass compositional group and in the intermediate region between the II and III compositional groups, respectively. While these compositions could suggest a Venetian origin, it is important to note that although the Venetian recipes were considered to be a guild secret, Venetian glass-makers travelled across Europe, opening their own glasshouses in Flanders

and London [128], making it impossible to pinpoint the production centers of these glasses based solely on their chemical glass type.

3.3.2. Glass provenance

The raw materials used to manufacture glass generally contain small amounts of impurities that are characteristic of the region from which they were obtained. Since glass composition reflects the chemical signature of the raw materials used in its manufacture, trace element analyses have been widely used to determine glass provenance (e.g. [14–16,18–22,24–26,41,129]).

An important amount of impurities is introduced via the silica source. Sand generally contains accessory minerals such as feldspars, zircon, aluminosilicates, Fe-Ti oxides and clay minerals [130]. Trace element distribution in particular can provide information on the silica source [20,24–26,129–131].

The chondrite-normalized [132] trace element composition (Figure 5) highlights the heterogeneity of the sands employed in the production of the glass beads in this study. Based on their compositional profiles, the beads have been subdivided into four groups. Group 1 is composed of the Venetian red and red-on-white glass beads (types 2, 3 or 4, 7, 10, 14 and 15), the white and pink stripes of the glass beads from type 17 and the white stripes from type 5. This group is characterized by having similar Rb and Sr values. The presence of only Venetian red, white and pink glass in this group is noteworthy as it suggests that the same raw material sources were used to make all these different colors.

The glass beads from Bohemia (types 12 and 13) constitute group 2. These beads have low Sr values, accompanied by high Rb values. The highest values of Zr and Hf can also be found in these glass beads. Rb^+ has an ionic radius similar to K^+ , which allows this element to be incorporated in the structure of K-bearing minerals such as clay-minerals or K-feldspars [133]. Zr and Hf on the other hand are most likely present in the heavy mineral zircon (ZrSiO_4), indicating that a mature sand, composed primarily of quartz, but with significant amounts of heavy minerals and an important clay fraction was used in the glass production [134].

Group 3 is composed exclusively of the Bavarian glass beads from type 1. These beads, like the ones in the previous group, are characterized by high Rb and low Sr values. However, they present the lowest values of Zr, Y and Hf. In general, low concentrations of trace elements indicate the use of high purity sand sources [130]. As previously mentioned, potash plant ash was used to manufacture these glass beads, which most likely resulted in the visible enrichment in Rb. The glass beads with unknown provenance and manufacture date types 16, 20, 22, 23, 24, 25, 46 and 47, as well as the green and reddish-brown glass from the type 5 Venetian glass beads, constitute group 4. This group is characterized by low Rb and high Sr values, accompanied by variable Ba amounts. The group has, therefore, been sub-divided into low Ba (group 4a) and high Ba (group 4b). Only the black beads from types 16, 20 and 23 constitute group 4b. While Ba could have been added unintentionally as an impurity in the silica source, a careful examination

of the LA-ICP-MS results revealed a correlation between Mn and Ba in these three bead types, suggesting that a mixture of pyrolusite (MnO_2) and psilomelane ($(\text{BaH}_2\text{O})_2\text{Mn}_5\text{O}_{10}$) was used to impart the black hue to the glass [130].

Two of the glass samples did not fit into any of the previously described compositional groups: the blue stripes of the type 17 glass beads, and the type 8 glass beads. The blue stripes of the 17 glass beads have a compositional profile similar to that of group 4a; however, this glass is greatly enriched in Y. The glass beads from type 8, on the other hand, present a compositional profile similar to that of group 3, but are enriched in Ba. As previously mentioned, the significant barium values found in the type 8 glass beads are most likely linked to the presence of barite in the silica source.

The largest portion of rare earth elements (REE) found in glass can be attributed to the silica source, as these elements occur in insignificant concentrations in both plant ash and carbonates [24]. The chondrite-normalized [132] rare earth element data revealed the presence of five groups of samples with different REE patterns (Figure 6 and Figure S2): groups A to E.

Despite the fact that REE usually have a uniform trivalent charge, Eu and Ce can be found in different oxidation states according to the redox conditions of the surrounding environment. Under reductive conditions, Eu assumes the bi-valence state, while Ce^{3+} becomes Ce^{4+} under oxidizing conditions. The Eu- and Ce-anomalies are, therefore, a measure of this redox-sensitive behavior[21], and fractionation relative to neighboring trivalent rare earth elements[135]. The formulas used to calculate the Eu- and Ce-anomalies can be found in Saitowitz (1996) and Robertshaw et al. (2006) [14,21].

Group A, which is similar to trace elements group 1, is composed of the Venetian glass beads from types 2, 3 or 4, 7, 10, 14, 15, and the pink and white stripes of type 17. The glass beads from type 46 which have unknown origin and manufacture date are also included in this group. Group A is characterized by an enrichment in light rare earth elements (LREEs) when compared to the high rare earth elements (HREEs) and negative Eu-anomalies ($\text{Eu}/\text{Eu}^* = 0.61-0.76$). A negative Eu-anomaly is formed by the separation of Eu^{2+} from Eu^{3+} in melts and the precipitation of Eu in its divalent state in plagioclase, substituting calcium. As sand inherits the Eu-anomaly from the source rock, the negative Eu-anomalies, in conjunction with the LREE enrichment, indicate the use of sand derived from the weathering of upper continental crust granite-type rocks[25,136].

Group B, which corresponds to trace element group 2, includes the Bohemian glass beads from types 12 and 13; it is characterized by a depletion of HREEs relative to LREEs and significant negative Eu-anomalies ($\text{Eu}/\text{Eu}^* = 0.31-0.41$). This group also has higher absolute REE abundance than Group A. The significant negative Eu-anomalies combined with the high REE absolute abundance indicate the use of sand sources that contain significant amounts of monazite and other REE minerals such as the Paleozoic and Mesozoic sandstones found in Germany and studied by Wedepohl et al. (2011) [25].

Group C, which corresponds to trace element group 3, is composed exclusively by the Bavarian glass beads from type 1. This group is also characterized by an enrichment in LREEs when compared to HREEs and negative Eu-anomalies ($\text{Eu}/\text{Eu}^* = 0.62$), indicating the use of sand derived from the weathering of upper continental crust rocks[25,136]. The lower absolute REE

abundance, when compared with Group A, might suggest the introduction of a sand purifying procedure to eliminate heavy minerals and clays, the minerals with the highest rare earth element abundance in sand [130].

Group D contains some of the glasses from the trace element group 4 such as the green and reddish-brown glass from the type 5 Venetian glass beads, as well as types 16, 20, 22 and 24 with unknown origin and manufacture date. This group has once again similar REE patterns to those of Group A, but with higher absolute REE abundance. It is characterized by a depletion of HREEs relative to LREEs and negative Eu-anomalies ($\text{Eu}/\text{Eu}^* = 0.65\text{-}0.76$). These REE patterns, in conjunction with the high REE abundance, suggest the use of immature sands derived from granite-type rocks.

Group E is composed of the white glass from the type 5 Venetian glass beads, as well as types 25 and 47 with unknown origin and manufacture date. This group is characterized by an enrichment in LREEs when compared to HREEs, but has Eu-anomalies with values closer to 1 ($\text{Eu}/\text{Eu}^* = 0.82\text{-}0.85$). The negative Eu-anomalies, combined with the LREE enrichment, indicate the use of sand resulting from the weathering of granite-type rocks[25,136].

Three of the glass samples did not fit into any of the previously described compositional groups: the glass beads from types 8 and 23, and the blue stripes of the Venetian type 17 glass beads. The glass beads from type 8 are characterized by having a very slight enrichment in LREEs relative to HREEs and the absence of an Eu-anomaly ($\text{Eu}/\text{Eu}^* = 1.0$). The glass beads from type 23 on the other hand, display similar REE patterns to those of Group D, but with negative Ce-anomalies ($\text{Ce}/\text{Ce}^* = 0.73$). The presence of negative Ce-anomalies in the glass beads from type 23 is most likely linked to the use of pyrolusite or psilomelane sources deriving from hydrothermal or diagenetic ferro-manganese crusts or nodules[137].

The REE pattern of the blue stripes of the Venetian type 17 glass beads shows an enrichment in middle rare earth elements (MREEs) when compared to the LREEs. This unusual REE pattern has been found, together with significant Y concentrations, in Egyptian and Mycenaean glass made from Egyptian cobalt-rich alum [129]. However, a careful examination of the LA-ICP-MS results revealed that cobalt was correlated with As, Ni, Bi, U and Fe, an association which is found in the Schneeberg region (Erzgebirge, Germany), while the cobalt-rich alum deposits of Egyptian origin have a chemical association of Co-Ni-Zn-Mg-Al [60]. This suggests the production of a synthetic cobalt-rich alum, most likely unintentionally obtained by using aluminosilicate-rich sands to produce *zaffera*, a cobalt blue glass coloring agent obtained by diluting a mixture of calcinated cobaltite and smaltite (from the Schneeberg mines) in siliceous sand [13].

4. Conclusions

A multi-analytical minimally invasive methodology was applied to study the morphology, the phase inclusions and the chemical composition of the glass bead assemblage found during the 2014 excavations carried out in the ruins of Kulumbimbi, Mbanza Kongo (Angola). The glass

beads were initially subjected to a careful typological classification. The micro-analytical approach that followed provided compositional data from the mono and multi-colored glass beads.

The chemical data indicates that the glass beads can be separated based on their fluxing agent source into three of the main glass types described by Gratuze & Janssens (2004) [60]: soda-lime plant ash glass, mixed alkali glass and potash-lime glass. All previously assigned Venetian glass beads can be described as soda-lime plant ash or mixed alkali glass. The high potassium concentrations found suggest that variable quality plant ash or a combination of *allume catina* and *gripola di vino* was being employed in the 18th to early 20th century Venetian glass bead production.

The major and trace element composition of the glass beads allowed the development of groups indicating different European provenances and different production methodologies (Table 4).

Table 4: Summary table highlighting the chemical composition and probable provenance of the glass bead types analyzed by LA-ICP-MS.

Bead type	Color	Fluxing agent	Trace element group	Rare earth element group	Probable provenance
1	Light blue	Potash-rich plant ash	Group 3	Group C	Bavaria
2	Red	Variable quality (mixed) plant ash	Group 1	Group A	Venice
3 or 4	Red	Variable quality (mixed) plant ash	Group 1	Group A	Venice
	White				
5	Green	Soda-rich plant ash	Group 4a	Group D	Venice
	Reddish-brown	Soda-rich plant ash	Group 4a	Group D	
	White	Soda-rich plant ash	Group 1	Group E	
7	Red	Variable quality (mixed) plant ash	Group 1	Group A	Venice
	White				
8	Blue	Potash-rich plant ash	Similar to group 3, but enriched in Ba	Absence of Eu-anomaly	Unknown, Central Europe?
10	Red	Variable quality (mixed) plant ash	Group 1	Group A	Venice
	White				
12	Blue	Potash-rich plant ash	Group 2	Group B	Bohemia
13	Blue	Potash-rich plant ash	Group 2	Group B	Bohemia
14	Red	Variable quality (mixed) plant ash	Group 1	Group A	Venice
	White				
15	Red	Variable quality (mixed) plant ash	Group 1	Group A	Venice
16	Black	Soda-rich plant ash	Group 4b	Group D	Venice
17	Pink	Variable quality (mixed) plant ash	Group 1	Group A	Venice
	White	Soda-rich plant ash	Group 1	Group A	
	Blue	Soda-rich plant ash	Similar to group 4a but with high Y values	Enrichment in MREEs	
20	Black	Soda-rich plant ash	Group 4b	Group D	Venice
22	Blue	Soda-rich plant ash	Group 4a	Group D	Venice

23	Black	Soda-rich plant ash	Group 4b	Negative Ce-anomalies	Unknown
24	Blue	Soda-rich plant ash	Group 4a	Group D	Venice
25	White	Soda-rich plant ash	Group 4a	Group E	Venice
46	Green	Soda-rich plant ash	Group 4a	Group A	Venice
47	White	Soda-rich plant ash	Group 4a	Group E	Venice

Lead arsenates and cassiterite were used to opacify the Venetian glass beads from types 2, 3 or 4, 6, 7, 9, 10, 11, 14, 15 and 19. Lead arsenates combined with lead stannate was also found in the type 5 glass beads. These opacifiers when combined with copper ions imparted an emerald green hue to the glass. Iron was found to be the chromophore responsible for the color of the reddish-brown stripes present in the type 5 glass beads, while VP-SEM-EDS revealed that cobalt was used to produce blue stripes found in the type 17 glass beads.

The chondrite-normalized rare earth element patterns revealed that the Venetian glass beads (Group A), which seem to have been fired at a temperature of approximately 800 °C, were made from a sand derived from the weathering of upper continental crust granite-type rocks. The chondrite-normalized trace element distribution, on the other hand, allowed the red, pink and white Venetian glass from types 2, 3 or 4, 7, 10, 14, 15 and 17 to be separated from the other glass hues. The higher Ca and Sr values found in the type 5 Venetian glass beads can be explained by the use of purer *allume catina*, as halophytic plant ash is enriched in calcium.

The blue glass beads from Central Europe (types 1, 12 and 13) were found to be composed of potash-lime plant ash glass. Handheld XRF data indicate that cobalt ions were used to produce the blue hues of the glass beads from types 1 and 13, while calcium phosphate was used as the main opacifying agent. Micro-Raman spectroscopy, on the other hand, revealed that the type 12 beads were fired at a temperature of around 1000 °C. LA-ICP-MS data showed that chondrite-normalized trace element distribution and chondrite-normalized REE patterns can be used to distinguish between the Bavarian (type 1) and the Bohemian (type 12 and 13) glass beads. The Bohemian glass beads seem to have been produced using a mature sand, composed primarily of quartz, but with significant amounts of heavy minerals such as monazite, while the Bavarian glass beads were manufactured using high purity sands.

Based on their chondrite-normalized trace element distribution and chondrite-normalized REE patterns the glass beads from types 16, 20, 22, 24, 25, 46 and 47, with previously unknown origin and manufacture date, are thought to have been produced in Venice. These glass beads also consist of soda-lime plant ash glass or mixed alkali glass, with variable potash contents, and high Ca and Sr values. Moreover, they seem to have been manufactured using sand derived from weathering of granite-type rocks and fired at temperatures between 800 and 1000 °C (values calculated for types 20, 22 and 24). The black beads from types 16 and 20, however, must be singled out due to their enrichment in Ba. The LA-ICP-MS results revealed a linear correlation between Mn and Ba in these glass bead types, suggesting that a mixture of pyrolusite (MnO₂) and psilomelane ((BaH₂O)₂Mn₅O₁₀) was used to impart the black hue to the glass. The type 16 glass

beads also show evidences of being composed of poor melting quality glass due to the identification of quartz and feldspar mineral phases by micro-Raman spectroscopy.

The origin of the glass beads from types 8 and 23 remain unknown. The blue glass beads from type 8 might have been produced in Central Europe since they can be characterized as potash-lime plant ash glass. However, they contain significant amounts of barium, suggesting the use of a barite-rich silica source, and very high As concentrations. These beads were opacified using calcium phosphate, and cobalt ions were used to produce the blue color.

The black type 23 glass beads were colored using a mixture of pyrolusite and psilomelane most likely originating from hydrothermal or diagenetic ferro-manganese crusts or nodules, as indicated by their negative Ce-anomaly. These beads were fired at a temperature between 800 and 1000 °C.

This archaeometric study shows that during the 17th-19th centuries, Mbanza Kongo was completely integrated in the Atlantic commerce routes with access to specific European beads productions. Therefore, the tombs of Kulumbimbi are also a window to an ancient African society closely connected to European societies.

Acknowledgments

The authors would like to thank the Angolan Government for funding the archaeological excavations carried out in the city of Mbanza Kongo during 2014 and the archaeological laboratory work conducted in 2015.

This work has been financially supported by a Concerted Research Action (GOA) of Ghent University, by Starting Grant No. 284126 of the European Research Council awarded to Koen Bostoen and by the Special Research Fund of Ghent University. The financial support of the Fundação para a Ciência e Tecnologia's (FCT) project UID/Multi/04449/2013, and the financial support given by the European Regional Development Fund through the COMPETE 2020 project POCI-01-0145-FEDER-007649, is also acknowledged. M. Costa also acknowledges FCT for a Ph.D. Fellowship (SFRH/BD/128889/2017).

References

- [1] J. Thornton, The Origins and Early History of the Kingdom of Kongo, c. 1350-1550, *Int. J. Afr. Hist. Stud.* 34 (2001) 89–120.
- [2] J.K. Thornton, The Origins of Kongo: A Revised Vision, in: K. Bostoen, I. Brinkman (Eds.), *Kongo Kingdom Orig. Dyn. Cosmop. Cult. an African Polity*, 1st ed., Cambridge University Press, Cambridge, UK, 2018: pp. 17–41.
- [3] B. Clist, E. Cranshof, G.-M. de Schryver, D. Herremans, K. Karklins, I. Matonda, F. Steyaert, K. Bostoen, African-European Contacts in the Kongo Kingdom (Sixteenth-Eighteenth Centuries): New Archaeological Insights from Ngongo Mbata (Lower Congo, DRC), *Int. J. Hist. Archaeol.* 19 (2015) 464–501. doi:10.1007/s10761-015-0296-3.

- [4] B. Clist, P. de Maret, K. Bostoen, eds., *Une archéologie des provinces septentrionales du royaume Kongo*, 1st ed., Archaeopress, Oxford, UK, 2018.
- [5] C.M. Radulet, *O cronista Rui de Pina e a “Relação do reino do Congo”*: manuscrito inédito do “Códice Riccardiano 1910,” Casa da Moeda, 1992.
- [6] J. Thornton, *Demography and History in the Kingdom of Kongo, 1550-1750*, Cambridge Univ. Press. 18 (1977) 507–530.
- [7] J.K. Thornton, *Mbanza Kongo/São Salvador: Kongo’s Holy City*, in: D. Anderson, R. Rathbone (Eds.), *Africa’s Urban Past*, James Currey, Oxford, 2000: pp. 67–84.
- [8] P. Batsikama, Á. Campelo, *A Catedral de São Salvador de Angola: história e memória de um lugar mítico*, *SÆculum - Rev. História*. 25 (2011) 161–179.
- [9] C.R. DeCorse, F.G. Richard, I. Thiaw, *Toward a Systematic Bead Description System: A View from the Lower Falemme, Senegal*, *J. African Archaeol.* 1 (2003) 77–109.
- [10] L.F. Stine, M.A. Cabak, M.D. Groover, *Blue Beads as African-American Cultural Symbols*, *Hist. Archaeol.* 30 (1996) 49–75.
- [11] K. Pallaver, ‘A recognized currency in beads’. *Glass Beads as Money in 19th-Century East Africa: the Central Caravan Road*, in: C. Eagleton, H. Fuller, J. Perkins (Eds.), *Africa’s Money in Africa*, The British Museum, 2009: pp. 20–29.
- [12] Z. Goffer, *Archaeological Chemistry*, John Wiley & Sons, Hoboken, 2007.
- [13] C. Moretti, S. Hreglich, *Raw Materials, Recipes and Procedures Used for Glass Making*, in: K. Janssens (Ed.), *Mod. Methods Anal. Archaeol. Hist. Glas. Vol. I*, John Wiley & Sons, Ltd, 2013: pp. 23–47. doi:10.1002/9781118314234.ch2.
- [14] S.J. Saitowitz, *Glass Beads as Indicators of Contact and Trade in Southern Africa ca. AD 900 - AD 1250*, University of Cape Town, 1996.
- [15] I. De Raedt, K. Janssens, J. Veeckman, L. Vincze, B. Vekemans, T.E. Jeffries, *Trace analysis for distinguishing between Venetian and façon-de-Venise glass vessels of the 16th and 17th century*, *J. Anal. At. Spectrom.* 16 (2001) 1012–1017. doi:10.1039/b102597j.
- [16] P. Robertshaw, M. Wood, A. Haour, K. Karklins, H. Neff, *Chemical analysis, chronology, and context of a European glass bead assemblage from Garumele, Niger*, *J. Archaeol. Sci.* 41 (2014) 591–604. doi:10.1016/j.jas.2013.08.023.
- [17] S. Conte, T. Chinni, R. Arletti, M. Vandini, *Butrint (Albania) between eastern and western Mediterranean glass production: EMPA and LA-ICP-MS of late antique and early medieval finds*, *J. Archaeol. Sci.* 49 (2014) 6–20. doi:10.1016/j.jas.2014.04.014.
- [18] M. Wood, S. Panighello, E.F. Orsega, P. Robertshaw, J.T. van Elteren, A. Crowther, M. Horton, N. Boivin, *Zanzibar and Indian Ocean trade in the first millennium CE: the glass bead evidence*, *Archaeol. Anthropol. Sci.* (2016) 1–23. doi:10.1007/s12520-015-0310-z.
- [19] P. Robertshaw, M.D. Glascock, M. Wood, R.S. Popelka, *Chemical analysis of ancient*

- African glass beads: a very preliminary report, *J. African Archaeol.* 1 (2003) 139–146. <http://www.jstor.org/stable/43134716>.
- [20] I.C. Freestone, The Provenance of Ancient Glass through Compositional Analysis, in: *Mater. Res. Soc. Symp. Proc.*, 2005: pp. 1–14.
- [21] P. Robertshaw, B. Rasoarifetra, M. Wood, E. Melchiorre, R.S. Popelka-Filcoff, M.D. Glascock, Chemical Analysis of Glass Beads from Madagascar, *J. African Archaeol.* 4 (2006) 91–109.
- [22] P. Robertshaw, S. Magnavita, M. Wood, E. Melchiorre, R. Popelka-Filcoff, M.D. Glascock, Glass Beads From Kissi (Burkina Faso): Chemical Analysis and Archaeological Interpretation, *J. African Archaeol. Monogr. Ser.* 2 (2009) 105–118.
- [23] P. Robertshaw, N. Benco, M. Wood, L. Dussubieux, E. Melchiorre, A. Ettahiri, Chemical Analysis Of Glass Beads From Medieval Al-Basra (Morocco), *Archaeometry.* 52 (2010) 355–379. doi:10.1111/j.1475-4754.2009.00482.x.
- [24] K.H. Wedepohl, K. Simon, A. Kronz, Data on 61 chemical elements for the characterization of three major glass compositions in Late Antiquity and the Middle Ages, *Archaeometry.* 53 (2011) 81–102. doi:10.1111/j.1475-4754.2010.00536.x.
- [25] K.H. Wedepohl, K. Simon, A. Kronz, The chemical composition including the Rare Earth Elements of the three major glass types of Europe and the Orient used in late antiquity and the Middle Ages, *Chemie Der Erde - Geochemistry.* 71 (2011) 289–296. doi:10.1016/j.chemer.2011.04.001.
- [26] M. Di Bella, S. Quartieri, G. Sabatino, F. Santalucia, M. Triscari, The glass mosaics tesserae of “Villa del Casale” (Piazza Armerina, Italy): a multi-technique archaeometric study, *Archaeol. Anthropol. Sci.* 6 (2014) 345–362. doi:10.1007/s12520-013-0172-1.
- [27] I. Kenyon, R.G.V. Hancock, S. Aufreiter, Neutron Activation Analysis of Ad 1660–1930 European Copper-Coloured Blue Glass Trade Beads From Ontario, Canada, *Archaeometry.* 37 (1995) 323–337. doi:10.1111/j.1475-4754.1995.tb00746.x.
- [28] R.G.V. Hancock, S. Aufreiter, I. Kenyon, European White Glass Trade Beads as Chronological and Trade Markers, *MRS Proc.* 462 (1997) 181–190. doi:10.1557/PROC-462-181.
- [29] R.G.V. Hancock, J. McKechnie, S. Aufreiter, K. Karklins, M. Kapches, M. Sempowski, J.F. Moreau, I. Kenyon, Non-destructive analysis of European cobalt blue glass trade beads, *J. Radioanal. Nucl. Chem.* 244 (2000) 567–573. doi:10.1023/A:1006705014455.
- [30] M.L. Sempowski, A.W. Nohe, R.G. V Hancock, J.-F. Moreau, F. Kwok, S. Aufreiter, K. Karklins, J. Baart, C. Garrad, I. Kenyon, Chemical analysis of 17th-century red glass trade beads from Northeastern North America and Amsterdam, *Archaeometry.* 43 (2001) 503–515. doi:10.1111/1475-4754.00033.
- [31] L.E. Burgess, L. Dussubieux, Chemical Composition of late 18th- and 19th-century glass beads from western North America: clues to sourcing beads, *BEADS J. Soc. Bead Res.*

- (2007) 58–73.
- [32] A. Shugar, A. O'Connor, The Analysis of 18th Century Glass Trade Beads from Fort Niagara: Insight into Compositional Variation and Manufacturing Techniques, *Northeast Hist. Archaeology*. 37 (2008) 58–68.
- [33] R.G.V. Hancock, European Glass Trade Beads in Northeastern North America, in: K. Janssens (Ed.), *Mod. Methods Anal. Archaeol. Hist. Glas.*, 2013: pp. 459–471.
- [34] L.C. Prinsloo, A. Tournié, P. Colomban, A Raman spectroscopic study of glass trade beads excavated at Mapungubwe hill and K2, two archaeological sites in southern Africa, raises questions about the last occupation date of the hill, *J. Archaeol. Sci.* 38 (2011) 3264–3277. doi:10.1016/j.jas.2011.07.004.
- [35] A. Tournié, L.C. Prinsloo, P. Colomban, Raman classification of glass beads excavated on Mapungubwe hill and K2, two archaeological sites in South Africa, *J. Raman Spectrosc.* 43 (2012) 532–542. doi:10.1002/jrs.3069.
- [36] A. Rousaki, A. Coccato, C. Verhaeghe, B. Clist, K. Bostoen, P. Vandenabeele, L. Moens, Combined Spectroscopic Analysis of Beads from the Tombs of Kindoki, Lower Congo Province (Democratic Republic of the Congo), *Appl. Spectrosc.* 70 (2016) 79–93. doi:10.1177/0003702815616595.
- [37] A. Coccato, M. Costa, A. Rousaki, B.-O. Clist, K. Karklins, K. Bostoen, A. Manhita, A. Cardoso, C. Barrocas Dias, A. Candeias, L. Moens, J. Mirão, P. Vandenabeele, Micro-Raman spectroscopy and complementary techniques (hXRF, VP-SEM-EDS, μ -FTIR and Py-GC/MS) applied to the study of beads from the Kongo Kingdom (Democratic Republic of the Congo), *J. Raman Spectrosc.* 48 (2017) 1468–1478. doi:10.1002/jrs.5106.
- [38] L. Dussubieux, B. Gratuze, M. Blet-Lemarquand, Mineral soda alumina glass: occurrence and meaning, *J. Archaeol. Sci.* 37 (2010) 1646–1655. doi:10.1016/j.jas.2010.01.025.
- [39] L. Dussubieux, C.M. Kusimba, V. Gogte, S.B. Kusimba, B. Gratuze, R. Oka, The trading of ancient glass beads: New analytical data from South Asian and East African soda-alumina glass beads, *Archaeometry*. 50 (2008) 797–821. doi:10.1111/j.1475-4754.2007.00350.x.
- [40] L.C. Prinsloo, P. Colomban, A Raman spectroscopic study of the Mapungubwe oblates: glass trade beads excavated at an Iron Age archaeological site in South Africa, *J. Raman Spectrosc.* 39 (2008) 79–90. doi:10.1002/jrs.
- [41] P. Robertshaw, M. Wood, E. Melchiorre, R.S. Popelka-Filcoff, M.D. Glascock, Southern African glass beads: chemistry, glass sources and patterns of trade, *J. Archaeol. Sci.* 37 (2010) 1898–1912. doi:10.1016/j.jas.2010.02.016.
- [42] D. Lauwers, A. Candeias, A. Coccato, J. Mirao, L. Moens, P. Vandenabeele, Evaluation of portable Raman spectroscopy and handheld X-ray fluorescence analysis (hXRF) for the direct analysis of glyptics, *Spectrochim. Acta - Part A Mol. Biomol. Spectrosc.* 157 (2016) 146–152. doi:10.1016/j.saa.2015.12.013.

- [43] B.O. Mysen, L.W. Finger, D. Virgo, F.A. Seifert, Curve-fitting of Raman spectra of silicate glasses, *Am. Mineral.* 67 (1982) 686–695.
- [44] P. Colomban, A. Tournié, L. Bellot-Gurlet, Raman identification of glassy silicates used in ceramics, glass and jewellery: a tentative, *J. Raman Spectrosc.* 37 (2006) 841–852. doi:10.1002/jrs.1515.
- [45] A. Cesaratto, P. Sichel, D. Bersani, P.P. Lottici, A. Montenero, E. Salvioli-Mariani, M. Catarsi, Characterization of archeological glasses by micro-Raman spectroscopy, *J. Raman Spectrosc.* 41 (2010) 1682–1687. doi:10.1002/jrs.2613.
- [46] B. Kirmizi, P. Colomban, M. Blanc, On-site analysis of Limoges enamels from sixteenth to nineteenth centuries: An attempt to differentiate between genuine artefacts and copies, *J. Raman Spectrosc.* 41 (2010) 1240–1247. doi:10.1002/jrs.2566.
- [47] N.J.G. Pearce, W.T. Perkins, J.A. Westgate, M.P. Gorton, S.E. Jackson, C.R. Neal, S.P. Chenery, A Compilation of New and Published Major and Trace Element Data for NIST SRM 610 and NIST SRM 612 Glass Reference Materials, *Geostand. Newsl. – J. Geostand. Geoanalysis.* 21 (1997) 115–144.
- [48] R.B. Scott, A.J. Shortland, P. Degryse, M. Power, K. Domoney, S. Boyen, D. Braekmans, In situ analysis of ancient glass: 17 th century painted glass from Christ Church Cathedral, Oxford and Roman glass vessels, *Glas. Technol. Eur. J. Glas. Sci. Technol. Part A.* 53 (2012) 65–73.
- [49] A. Bonneau, J. Moreau, R.G. V Hancock, K. Karklins, Archaeometrical Analysis of Glass Beads: Potential, Limitations, and Results, *BEADS J. Soc. Bead Res.* 26 (2014) 35–46.
- [50] R.B. Scott, K. Eekelers, L. Fredericks, P. Degryse, A methodology for qualitative archaeometallurgical fieldwork using a handheld X-ray fluorescence spectrometer, *STAR Sci. Technol. Archaeol. Res.* 1 (2016) 70–80. doi:10.1080/20548923.2016.1183941.
- [51] C.N. Duckworth, J. Henderson, F.J.M. Rutten, K. Nikita, Opacifiers in Late Bronze Age glasses: The use of ToF-SIMS to identify raw ingredients and production techniques, *J. Archaeol. Sci.* 39 (2012) 2143–2152. doi:10.1016/j.jas.2012.02.011.
- [52] H. Bronk, S. Röhrs, A. Bjeoumikhov, N. Langhoff, J. Schmalz, R. Wedell, H.E. Gorny, A. Herold, U. Waldschläger, ArtTAX - A new mobile spectrometer for energy-dispersive micro X-ray fluorescence spectrometry on art and archaeological objects, *Fresenius. J. Anal. Chem.* 371 (2001) 307–316. doi:10.1007/s002160100989.
- [53] M. Mantler, M. Schreiner, X-ray analysis of objects of art and archaeology, *J. Radioanal. Nucl. Chem.* 247 (2001) 635–644. doi:10.1023/A:1010671619353.
- [54] P.J. Potts, F. Bernardini, M.C. Jones, O. Williams-Thorpe, P.C. Webb, Effects of weathering on in situ portable X-ray fluorescence analyses of geological outcrops: Dolerite and rhyolite outcrops from the Preseli Mountains, South Wales, *X-Ray Spectrom.* 35 (2006) 8–18. doi:10.1002/xrs.881.
- [55] P. Mirti, P. Davit, M. Gulmini, Colourants and opacifiers in seventh and eighth century

- glass investigated by spectroscopic techniques, *Anal. Bioanal. Chem.* 372 (2002) 221–229. doi:10.1007/s00216-001-1183-9.
- [56] A.M. Pollard, C. Heron, *Archaeological Chemistry, Second*, The Royal Society of Chemistry, Cambridge, UK, 2008.
- [57] A. Lima, T. Medici, A. Pires de Matos, M. Verità, Chemical analysis of 17th century Millefiori glasses excavated in the Monastery of Sta. Clara-a-Velha, Portugal: comparison with Venetian and façon-de-Venise production, *J. Archaeol. Sci.* 39 (2012) 1238–1248. doi:10.1016/j.jas.2012.01.006.
- [58] M. Verità, A. Renier, S. Zecchin, Chemical analyses of ancient glass findings excavated in the Venetian lagoon, *J. Cult. Herit.* 3 (2002) 261–271. doi:10.1016/S1296-2074(02)01235-9.
- [59] A.J. Shortland, The use and origin of antimonate colorants in early Egyptian glass, *Archaeometry.* 44 (2002) 517–530. doi:10.1111/1475-4754.t01-1-00083.
- [60] B. Gratuze, K. Janssens, Provenance analysis of glass artefacts, in: K. Janssens, R. Van Grieken (Eds.), *Compr. Anal. Chem.*, 1st ed., Elsevier Science, 2004: pp. 663–712. doi:10.1016/S0166-526X(04)80019-9.
- [61] F. Licenziati, T. Calligaro, Study of mosaic glass tesserae from Delos, Greece using a combination of portable micro-Raman and X-ray fluorescence spectrometry, *J. Archaeol. Sci. Reports.* 7 (2016) 640–648. doi:10.1016/j.jasrep.2015.10.017.
- [62] D. Möncke, M. Papageorgiou, A. Winterstein-Beckmann, N. Zacharias, Roman glasses coloured by dissolved transition metal ions: Redox-reactions, optical spectroscopy and ligand field theory, *J. Archaeol. Sci.* 46 (2014) 23–36. doi:10.1016/j.jas.2014.03.007.
- [63] G.V. Rao, Nickel and Cobalt Ores: Flotation, *Encycl. Sep. Sci. Acad. Press. New York.* (2000) 3491–3500. doi:10.1016/B978-0-12-409547-2.10944-8.
- [64] B. Gratuze, I. Soulier, J.-N. Barrandon, D. Foy, De l'origine du cobalt dans les verres., *Rev. d'archéométrie.* 16 (1992) 97–108. doi:10.3406/arsci.1992.895.
- [65] B. Gratuze, I. Soulier, M. Blet, L. Vallauri, De l'origine du cobalt: du verre à la céramique, *Rev. d'archéométrie.* (1996) 77–94. doi:10.3406/arsci.1996.939.
- [66] A. Zucchiatti, L. Canonica, P. Prati, A. Cagnana, S. Roascio, A.C. Font, PIXE analysis of V-XVI century glasses from the archaeological site of San Martino di Ovaro (Italy), *J. Cult. Herit.* 8 (2007) 307–314. doi:10.1016/j.culher.2007.05.003.
- [67] T. Calligaro, PIXE in the study of archaeological and historical glass, *X-Ray Spectrom.* 37 (2008) 169–177. doi:10.1002/xrs.1063 PIXE.
- [68] J.E. Dayton, Geological evidence for the discovery of cobalt blue glass in Mycenaean times as a by-product of silver smelting in the Schneeberg area of the Bohemian Erzgebirge, *Rev. d'archeometrie.* 1 (1981) 57–61.

- [69] E.S. Bastin, The nickel-cobalt-native silver ore type, *Econ. Geol.* 34 (1939) 1–40. doi:10.2113/gsecongeo.34.1.1.
- [70] L. Robinet, C. Coupry, K. Eremin, C. Hall, Raman investigation of the structural changes during alteration of historic glasses by organic pollutants, *J. Raman Spectrosc.* 37 (2006) 1278–1286. doi:10.1002/jrs.1549.
- [71] A. Silvestri, F. Nestola, L. Peruzzo, Multi-methodological characterisation of calcium phosphate in late-Antique glass mosaic tesserae, *Microchem. J.* 124 (2016) 811–818. doi:10.1016/j.microc.2015.10.026.
- [72] R. Kresse, U. Baudis, P. Jäger, H.H. Riechers, H. Wagner, J. Winkler, H.U. Wolf, Barium and barium compounds, *Ullmann's Encycl. Ind.* 4 (2012) 621–640. doi:10.1002/14356007.a03_325.pub2.
- [73] K.H. Wedepohl, a Baumann, The use of marine molluscan shells for Roman glass and local raw glass production in the Eifel area (western Germany)., *Naturwissenschaften.* 87 (2000) 129–132. doi:10.1007/s001140050690.
- [74] S.E. Campana, Chemistry and composition of fish otoliths: pathways, mechanisms and applications, *Mar. Ecol. Prog. Ser.* 188 (1999) 263–297. doi:10.3354/meps188263.
- [75] R.Z. LeGeros, O.R. Trautz, E. Klein, J.P. LeGeros, Two types of carbonate substitution in the apatite structure, *Experientia.* 25 (1969) 5–7. doi:10.1007/BF01903856.
- [76] M. Tite, T. Pradell, A.J. Shortland, Discovery, production and use of tin-based opacifiers in glasses, enamels and glazes from the Late Iron Age onwards: A reassessment, *Archaeometry.* 50 (2008) 67–84. doi:10.1111/j.1475-4754.2007.00339.x.
- [77] P. Colomban, The Use of Metal Nanoparticles to Produce Yellow, Red and Iridescent Colour, from Bronze Age to Present Times in Lustre Pottery and Glass: Solid State Chemistry, Spectroscopy and Nanostructure, *J. Nano Res.* 8 (2009) 109–132. doi:10.4028/www.scientific.net/JNanoR.8.109.
- [78] P. Mirti, A. Lepora, L. Sagui, Scientific analysis of seventh-century glass fragments from the Crypta Balbi in Rome, *Archaeometry.* 42 (2000) 359–374. doi:10.1111/j.1475-4754.2000.tb00887.x.
- [79] R. Arletti, M.C. Dalconi, S. Quartieri, M. Triscari, G. Vezzalini, Roman coloured and opaque glass: A chemical and spectroscopic study, *Appl. Phys. A Mater. Sci. Process.* 83 (2006) 239–245. doi:10.1007/s00339-006-3515-2.
- [80] M. Verità, M.S. Arena, A.M. Carruba, P. Santopadre, Roman glass: Art and technology in a 4th century A.D. opus sectile in Ostia (Rome), *J. Cult. Herit.* 9 (2008) 16–20. doi:10.1016/j.culher.2008.08.004.
- [81] R. Feller, ed., *Artist's pigments: a handbook of their history and characteristics. Volume 1*, National Gallery of Art and Archetype Publications Ltd., 1986.
- [82] M. Thoury, J.K. Delaney, E. René de la Rie, M. Palmer, K. Morales, J. Krueger, Near-

- Infrared Luminescence of Cadmium Pigments : In Situ Identification and Mapping in Paintings, *Appl. Spectrosc.* 65 (2011) 939–951. doi:10.1366/11-06230.
- [83] L.C. Prinsloo, J.C.A. Boeyens, M.M. van der Ryst, G. Webb, Raman signatures of the modern pigment (Zn,Cd) $S_{1-x}Se_x$ and glass matrix of a red bead from Magoro Hill, an archaeological site in Limpopo Province, South Africa, recalibrate the settlement chronology, *J. Mol. Struct.* 1023 (2012) 123–127. doi:10.1016/j.molstruc.2012.03.047.
- [84] M. Bouchard, D.C. Smith, C. Carabatos-Nédelec, An investigation of the feasibility of applying Raman microscopy for exploring stained glass, *Spectrochim. Acta - Part A Mol. Biomol. Spectrosc.* 68 (2007) 1101–1113. doi:10.1016/j.saa.2007.06.045.
- [85] P. Ricciardi, P. Colomban, A. Tournié, V. Milande, Nondestructive on-site identification of ancient glasses: genuine artefacts, embellished pieces or forgeries?, *J. Raman Spectrosc.* 40 (2009) 604–617. doi:10.1002/jrs.2165.
- [86] M. Verità, L. James, I. Freestone, J. Henderson, M.-D. Nenna, N. Schibille, Glossary of mosaic glass terms, *Humanities.* 1273 (2009) 678001.
- [87] S. Röhrs, H. Stege, Analysis of Limoges painted enamels from the 16th to 19th centuries by using a portable micro x-ray fluorescence spectrometer, *X-Ray Spectrom.* 33 (2004) 396–401. doi:10.1002/xrs.713.
- [88] B. Velde, Glass Compositions over Several Millennia in the Western World, in: K. Janssens (Ed.), *Mod. Methods Anal. Archaeol. Hist. Glas. Vol. I*, John Wiley & Sons, Ltd, 2013: pp. 67–78.
- [89] S. La Delfa, E. Ciliberto, L. Pirri, Behaviour of copper and lead as chromophore elements in sodium silicate glasses, *J. Cult. Herit.* 9 (2008) e117–e122. doi:10.1016/j.culher.2008.07.006.
- [90] I. Biron, M. Verità, Analytical investigation on Renaissance Venetian enamelled glasses from the Louvre collections, *J. Archaeol. Sci.* 39 (2012) 2706–2713. doi:10.1016/j.jas.2012.03.014.
- [91] S. Lahlil, M. Cotte, I. Biron, J. Szlachetko, N. Menguye, J. Susinib, Synthesizing lead antimonate in ancient and modern opaque glass, *J. Anal. At. Spectrom.* 26 (2011) 1040–1050. doi:10.1039/c0ja00251h.
- [92] C. Cascales, J.A. Alonso, I. Rasines, The new pyrochlores $Pb_2(MSb)O_{6.5}$ ($M = Ti, Zr, Sn, Hf$), *J. Mater. Sci. Lett.* 5 (1986) 675–677.
- [93] S. Lahlil, I. Biron, L. Galois, G. Morin, Rediscovering ancient glass technologies through the examination of opacifier crystals, *Appl. Phys. A Mater. Sci. Process.* 92 (2008) 109–116. doi:10.1007/s00339-008-4456-8.
- [94] E. Basso, C. Invernizzi, M. Malagodi, M.F. La Russa, D. Bersani, P.P. Lottici, Characterization of colorants and opacifiers in roman glass mosaic tesserae through spectroscopic and spectrometric techniques, *J. Raman Spectrosc.* 45 (2014) 238–245. doi:10.1002/jrs.4449.

- [95] V.S.F. Muralha, S. Canaveira, J. Mirão, S. Coentro, T. Morna, C. Stefano, Baroque glass mosaics from the Capela de São João Baptista (Chapel of Saint John the Baptist, Lisbon): unveiling the glassmaking records, *J. Raman Spectrosc.* 48 (2015) 483–492. doi:10.1002/jrs.4669.
- [96] F. Rosi, V. Manuali, C. Miliani, B.G. Brunetti, A. Sgamellotti, T. Grygar, D. Hradil, Raman scattering features of lead pyroantimonate compounds . Part I : XRD and Raman characterization of Pb₂Sb₂O₇ doped with tin and zinc, *J. Ram.* 40 (2009) 107–111. doi:10.1002/jrs.2092.
- [97] M. Verità, Secrets and Innovations of Venetian Glass Between the 15th and the 17th Centuries: Raw Materials, Glass Melting and Artefacts, in: R. Barovier, C. Tonini (Eds.), *Study Days Venetian Glas. Approx. 1600's*, Istituto Veneto di Scienze, Lettere ed Arti, 2014: pp. 53–68.
- [98] A. Roy, B.H. Berrie, A new lead-based yellow in the seventeenth century, *Paint. Tech. Hist. Mater. Stud. Pract. Contrib. to Dublin Congr.* 7-11 Sept. 1998. 3630 (1998) 3–10. doi:10.1179/sic.1998.43.Supplement-1.160.
- [99] M. Di Bella, C. Giacobbe, S. Quartieri, G. Sabatino, U. Spigo, Archaeometric characterization of Proto-Byzantine glass workshop from the Roman amphitheatre of Catania (Sicily, Italy), *Eur. J. Mineral.* 27 (2015) 353–363. doi:10.1127/ejm/2015/0027-2449.
- [100] E. Gliozzo, M. Turchiano, F. Giannetti, I. Memmi, Late Antique and Early Medieval Glass Vessels from Faragola (Italy), *Archaeometry.* 58 (2016) 113–147. doi:10.1111/arcm.12242.
- [101] P. Colomban, Polymerization degree and Raman identification of ancient glasses used for jewelry, ceramic enamels and mosaics, *J. Non. Cryst. Solids.* 323 (2003) 180–187. doi:10.1016/S0022-3093(03)00303-X.
- [102] P. Colomban, Raman spectrometry, a unique tool to analyze and classify ancient ceramics and glasses, *Appl. Phys. A Mater. Sci. Process.* 79 (2004) 167–170. doi:10.1007/s00339-004-2512-6.
- [103] P. Ricciardi, P. Colomban, A. Tournié, M. Macchiarola, N. Ayed, A non-invasive study of Roman Age mosaic glass tesserae by means of Raman spectroscopy, *J. Archaeol. Sci.* 36 (2009) 2551–2559. doi:10.1016/j.jas.2009.07.008.
- [104] H.X. Zhao, Q.H. Li, S. Liu, F.X. Gan, Characterization of microcrystals in some ancient glass beads from china by means of confocal Raman microspectroscopy, *J. Raman Spectrosc.* 44 (2013) 643–649. doi:10.1002/jrs.4239.
- [105] Y. Batonneau, C. Brémard, J. Laureyns, J.C. Merlin, Microscopic and imaging Raman scattering study of PbS and its photo-oxidation products, *J. Raman Spectrosc.* 31 (2000) 1113–1119.
- [106] J.G. Shapter, M.H. Brooker, W.M. Skinner, Observation of the oxidation of galena using Raman spectroscopy, *Int. J. Miner. Process.* 60 (2000) 199–211.

- [107] L. Burgio, R.J.H. Clark, S. Firth, Raman spectroscopy as a means for the identification of plattnerite (PbO₂), of lead pigments and of their degradation products, *Analyst*. 126 (2001) 222–227. doi:10.1039/b008302j.
- [108] A.M. Correia, R.J.H. Clark, M.I.M. Ribeiro, M.L.T.S. Duarte, Pigment study by Raman microscopy of 23 paintings by the Portuguese artist Henrique Pousão (1859–1884), *J. Raman Spectrosc.* 38 (2007) 1390–1405. doi:10.1002/jrs.1786.
- [109] M.L. Frezzotti, F. Tecce, A. Casagli, Raman spectroscopy for fluid inclusion analysis, *J. Geochemical Explor.* 112 (2012) 1–20. doi:10.1016/j.gexplo.2011.09.009.
- [110] G. Penel, G. Leroy, C. Rey, E. Bres, MicroRaman Spectral Study of the PO₄ and CO₃ Vibrational Modes in Synthetic and Biological Apatites, *Calcif. Tissue Int.* 63 (1998) 475–481. doi:10.1007/s002239900561.
- [111] N. Welter, U. Schussler, W. Kiefer, Characterisation of inorganic pigments in ancient glass beads by means of Raman microspectroscopy, microprobe analysis and X-ray diffractometry, *J. Raman Spectrosc.* 38 (2007) 113–121. doi:10.1002/jrs.
- [112] S. Andrò, E. Garzanti, Raman spectroscopy in heavy-mineral studies, in: R.A. Scott, H.R. Smyth, A.C. Morton, N. Richardson (Eds.), *Sediment Proven. Stud. Hydrocarb. Explor. Prod.*, Geological Society, Special Publications, London, 2016: pp. 395–412. doi:10.1144/SP386.2.
- [113] G. Bartholomäi, W.E. Klee, The vibrational spectra of pyromorphite, vanadinite and mimetite, *Spectrochim. Acta Part A Mol. Spectrosc.* 34 (1978) 831–843. doi:10.1016/0584-8539(78)80038-5.
- [114] L.R. Ong, E. Widjaja, R. Stanforth, M. Garland, Fourier transform Raman spectral reconstruction of inorganic lead mixtures using a novel band-target entropy minimization (BTEM) method, *J. Raman Spectrosc.* 34 (2003) 282–289. doi:10.1002/jrs.986.
- [115] C. Miguel, A. Claro, A.P. Gonçalves, V.S.F. Muralha, M.J. Melo, A study on red lead degradation in a medieval manuscript *Lorvão Apocalypse* (1189), *J. Raman Spectrosc.* 40 (2009) 1966–1973. doi:10.1002/jrs.2350.
- [116] J. Van Pevenage, D. Lauwers, D. Herremans, E. Verhaeven, B. Vekemans, W. De Clercq, L. Vincze, L. Moens, P. Vandennebeele, A combined spectroscopic study on Chinese porcelain containing ruan-cai colours, *Anal. Methods*. 6 (2014) 387–394. doi:10.1039/c3ay41072b.
- [117] R.L. Frost, P.A. Williams, W. Martens, P. Leverett, J.T. Kloprogge, Raman spectroscopy of basic copper (II) and some complex copper (II) sulfate minerals: Implications for hydrogen bonding, *Am. Mineral.* 89 (2004) 1130–1137.
- [118] T. Ohsaka, S. Yamaoka, Effect of hydrostatic pressure on the raman spectrum of anatase (TiO₂), *Solid State Commun.* 30 (1979) 345–347. doi:10.1016/0038-1098(79)90648-3.
- [119] U. Balachandran, N.G. Eror, Raman Spectra of Titanium Dioxide, *J. Solid State Chem.* 42 (1982) 276–282.

- [120] G.A. Tompsett, G.A. Bowmaker, R.P. Cooney, J.B. Metson, K.A. Rodgers, J.M. Seakins, The Raman spectrum of brookite, TiO_2 (Pbca, $Z = 8$), *J. Raman Spectrosc.* 26 (1995) 57–62. doi:10.1002/jrs.1250260110.
- [121] H.G.M. Edwards, Analytical Raman spectroscopic discrimination between yellow pigments of the Renaissance, *Spectrochim. Acta. A. Mol. Biomol. Spectrosc.* 80 (2011) 14–20. doi:10.1016/j.saa.2010.12.023.
- [122] M.A. Cortés-Jácome, G. Ferrat-Torres, L.F.F. Ortiz, C. Angeles-Chávez, E. López-Salinas, J. Escobar, M.L. Mosqueira, J.A. Toledo-Antonio, In situ thermo-Raman study of titanium oxide nanotubes, *Catal. Today.* 126 (2007) 248–255. doi:10.1016/j.cattod.2007.02.012.
- [123] R.J.H. Clark, L. Cridland, B.M. Kariuki, K.D.M. Harris, R. Withnall, Synthesis, Structural Characterisation and Raman Spectroscopy of the Inorganic Pigments Lead Tin Yellow Types I and II and Lead Antimonate Yellow: Their Identification on Medieval Paintings and Manuscripts, *J. Chem. Soc. Dalt. Trans.* (1995) 2577–2582. doi:10.1039/DT9950002577.
- [124] I.M. Bell, R.J.H. Clark, P.J. Gibbs, Raman spectroscopic library of natural and synthetic pigments (Pre- ~ 1850 AD), *Spectrochim. Acta - Part B At. Spectrosc.* 53 (1997) 2159–2179.
- [125] S. Cagno, L. Favaretto, M. Mendera, A. Izmer, F. Vanhaecke, K. Janssens, Evidence of early medieval soda ash glass in the archaeological site of San Genesio (Tuscany), *J. Archaeol. Sci.* 39 (2012) 1540–1552. doi:10.1016/j.jas.2011.12.031.
- [126] S. Cagno, P. Cosyns, A. Izmer, F. Vanhaecke, K. Nys, K. Janssens, Deeply colored and black-appearing Roman glass: A continued research, *J. Archaeol. Sci.* 42 (2014) 128–139. doi:10.1016/j.jas.2013.11.003.
- [127] S.C. Rasmussen, *How Glass Changed the World: The History and Chemistry of Glass from Antiquity to the 13th century*, Springer, 2012.
- [128] K. Janssens, S. Cagno, I. De Raedt, P. Degryse, *Transfer of Glass Manufacturing Technology in the Sixteenth and Seventeenth Centuries from Southern to Northern Europe: Using Trace Element Patterns to Reveal the Spread from Venice via Antwerp to London*, John Wiley & Sons, Ltd., 2013. doi:10.1002/9781118314234.ch25.
- [129] S. Conte, R. Arletti, F. Mermati, B. Gratuze, Unravelling the Iron Age glass trade in southern Italy: the first trace-element analyses, *Eur. J. Mineral.* 28 (2016) 409–433. doi:10.1127/ejm/2016/0028-2516.
- [130] D. Brems, P. Degryse, Trace element analysis in provenancing Roman glass-making, *Archaeometry.* 56 (2014) 116–136. doi:10.1111/arcms.12063.
- [131] K.H. Wedepohl, K. Simon, The chemical composition of medieval wood ash glass from Central Europe, *Chemie Der Erde - Geochemistry.* 70 (2010) 89–97. doi:10.1016/j.chemer.2009.12.006.
- [132] W.F. McDonough, S. -s. Sun, The composition of the Earth, *Chem. Geol. (Isotope Geosci.*

Sect. 120 (1995) 223–253.

- [133] D.G. Brookins, *Geochemical Aspects of Radioactive Waste Disposal*, Springer-Verlag, New York, 1984. doi:10.1007/978-1-4613-8254-6.
- [134] D. Barca, E. Basso, D. Bersani, G. Galli, C. Invernizzi, M.F. La Russa, P.P. Lottici, M. Malagodi, S.A. Ruffolo, Vitreous tesserae from the calidarium mosaics of the Villa dei Quintili, Rome. Chemical composition and production technology, *Microchem. J.* 124 (2016) 726–735. doi:10.1016/j.microc.2015.10.037.
- [135] M. Seto, T. Akagi, Chemical condition for the appearance of a negative Ce anomaly in stream waters and groundwaters, *Geochem. J.* 42 (2008) 371–380. doi:10.2343/geochemj.42.371.
- [136] W.M. White, *Geochemistry*, Blackwell-Wiley, Oxford, 2013.
- [137] M. Bau, K. Schmidt, A. Koschinsky, J. Hein, T. Kuhn, A. Usui, Discriminating between different genetic types of marine ferro-manganese crusts and nodules based on rare earth elements and yttrium, *Chem. Geol.* 381 (2014) 1–9. doi:10.1016/j.chemgeo.2014.05.004.

Figure captions:

Figure 1: a) Ruins of Kulumbimbi (Mbanza Kongo, Angola) in 2014; b) detailed image of the female remains found in burial 1. This 22-year-old woman had almost 3000 beads around her neck, wrists and ankles.

Figure 2: a) hXRF Co-Cu plot indicating that the blue glass beads from types 1, 8, 12, 13 and 22 are enriched in Co, while the blue type 24 glass beads are enriched in Co and Cu; b) hXRF Pb-As plot indicating that both Pb and As were used in the production of the glass beads from types 2, 3 or 4, 5, 6, 7, 9, 10, 11, 14, 15, 17 and 19; c) hXRF Sb-Ca evidencing that the glass beads from types 22, 25, 46 and 47 are simultaneously enriched in Sb and Ca; d) hXRF Pb-Sn plot showing the combined use of Pb and Sn to opacify the type 5 glass beads; e) hXRF Mn-Fe plot corroborating the use of these two elements in the production of the black type 16, 20 and 23 glass beads; f) hXRF Cu-Fe plot substantiating the use of Cu and Fe to produce the green glass present in the type 5 and 46 glass beads.

Figure 3: a) VP-SEM image of the type 25 glass beads. The white areas were found to be calcium antimonate aggregates; b) point analysis of one of the calcium antimonate aggregates.

Figure 4: Ternary diagram of the normalized Na_2O , $\text{MgO} + \text{K}_2\text{O}$ and CaO contents of the glass beads analyzed by LA-ICP-MS. Four main chemical glass types are evidenced by the ellipses [60].

Figure 5: Chondrite-normalized [132] trace element composition of the glass beads analyzed by LA-ICP-MS. A detailed explanation of the different groups can be found in the text.

Figure 6: Chondrite-normalized [132] representative REE patterns of the glass beads analyzed by LA-ICP-MS. A detailed explanation of the different groups can be found in the text.

Captions for supplementary material:

Figure S1: hXRF bi-plots. a) Co-Ni; b) Co-As; c) Zn-Co; d) Pb-Co; e) Co-Fe; f) Cr-Co; g) Bi-Co; h) Ca-Ba.

Figure S2: Chondrite-normalized [132] REE patterns of the glass beads analyzed by LA-ICP-MS.

Table S1: Overview of the glass beads studied, including typology, tombs in which they were found, untested possible origin and date, manufacture technique, color and size.

Table S2: Representative composition of each glass bead type acquired by VP-SEM-EDS.

Table S3: Average values of REE and other trace elements (Ti, V, Cr, Rb, Sr, Y, Zr, Nb, Ba, Hf, Ta and Th) determined by LA-ICP-MS. Both non-normalized and chondrite-normalized values are included.

ACCEPTED MANUSCRIPT

Highlights

- Application of multi-analytical minimally invasive methodology, which includes hXRF, VP-SEM-EDS, micro-Raman spectroscopy and LA-ICP-MS to the study of several glass bead assemblages.
- Determination of the coloring and opacifying agents used in the manufacture of each glass bead type.
- Use of trace element analysis to identify the main production regions of each glass bead type.

ACCEPTED MANUSCRIPT



Figure 1

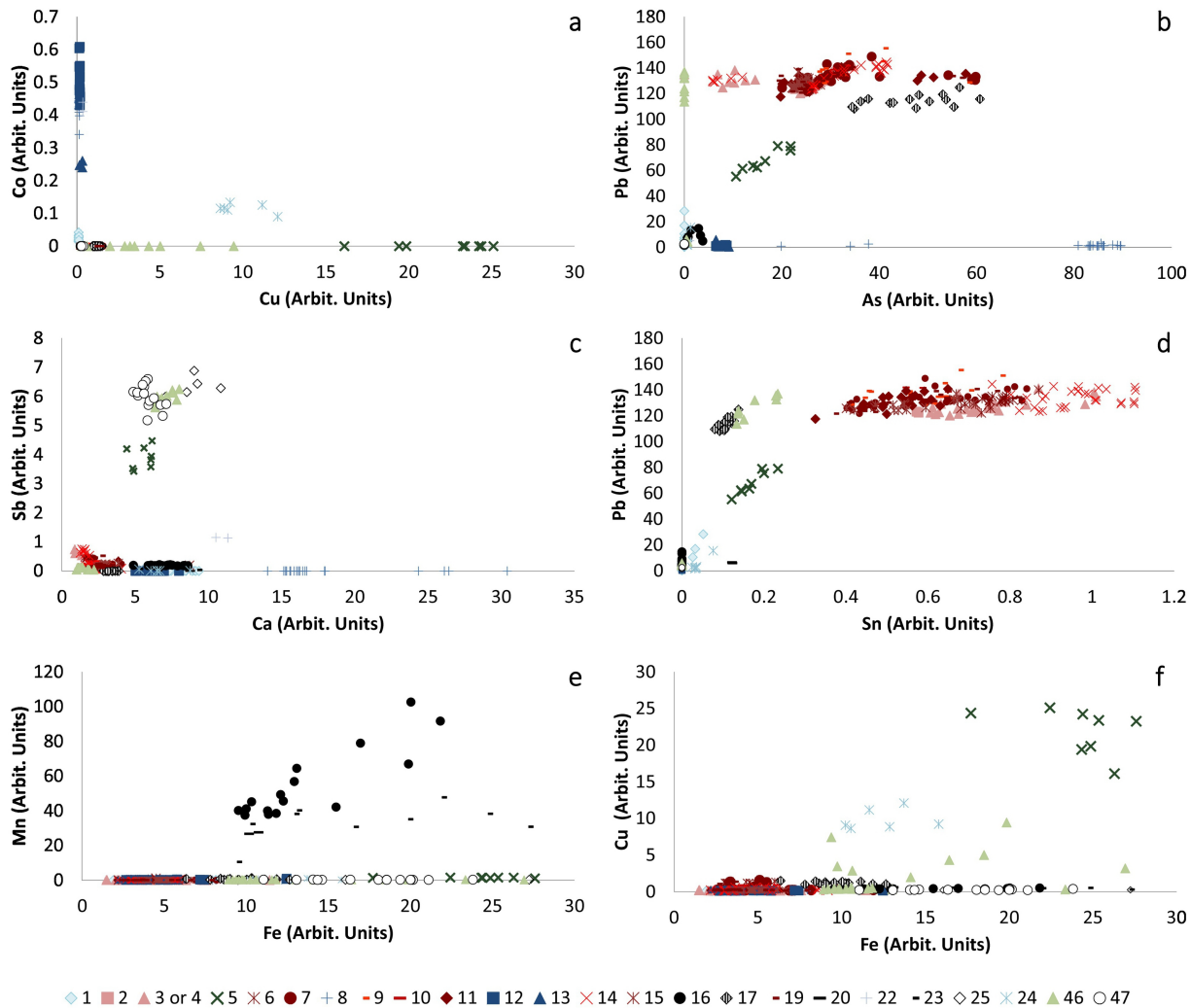


Figure 2

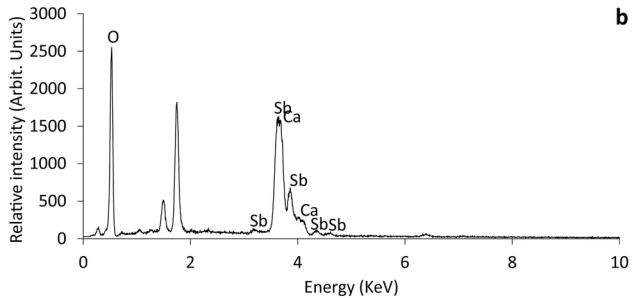
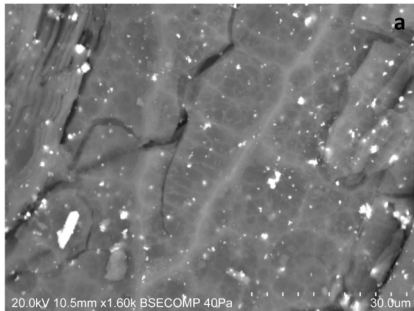


Figure 3

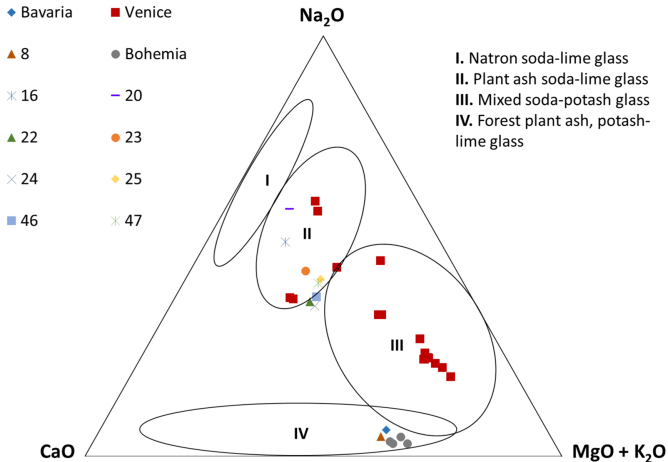


Figure 4

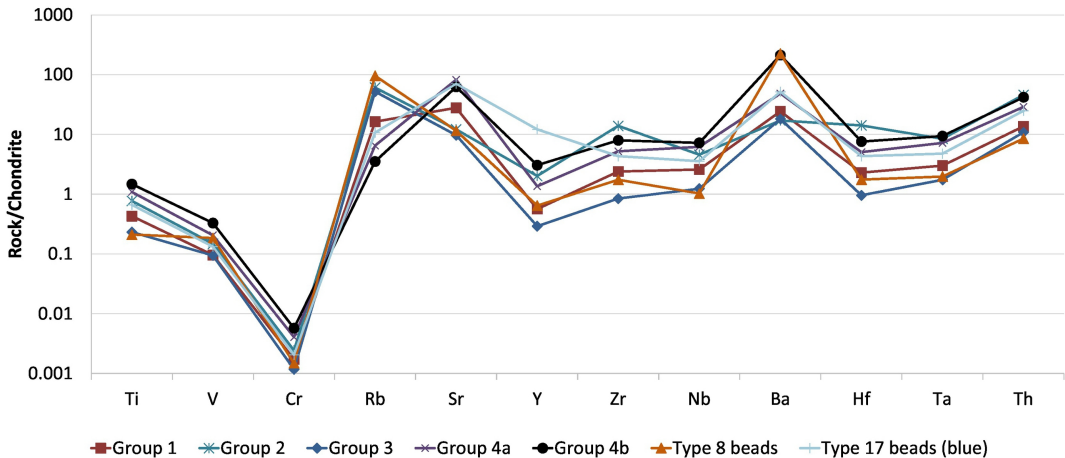


Figure 5

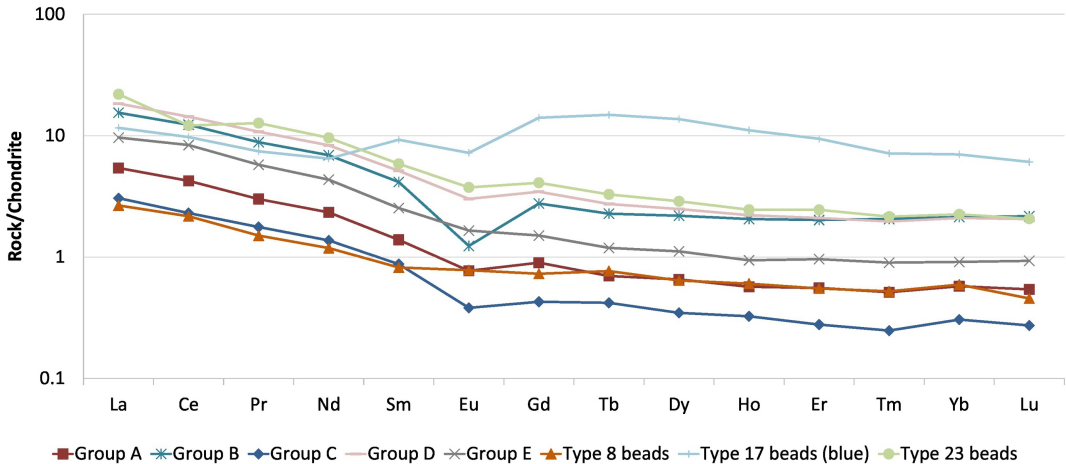


Figure 6

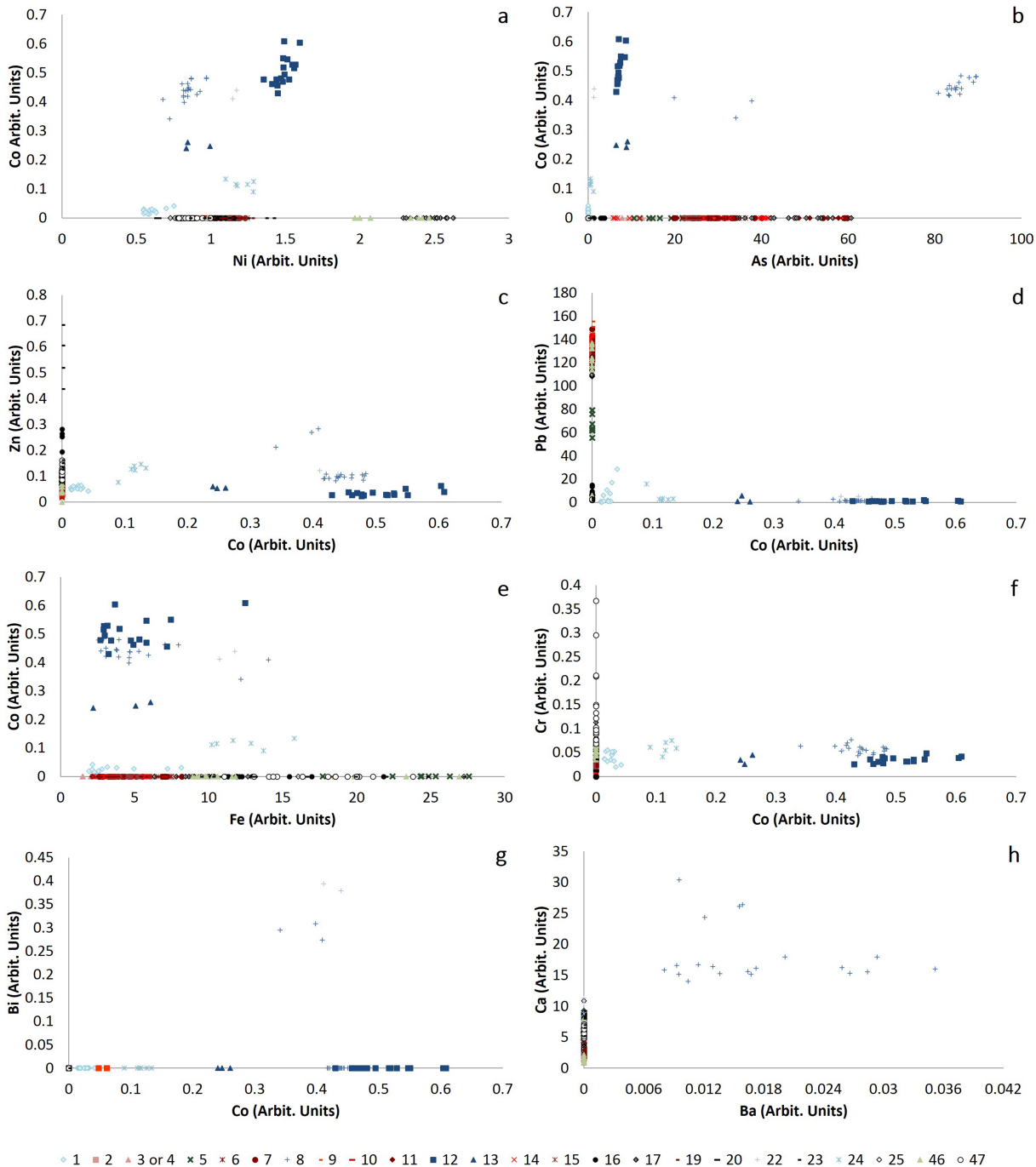


Figure 7

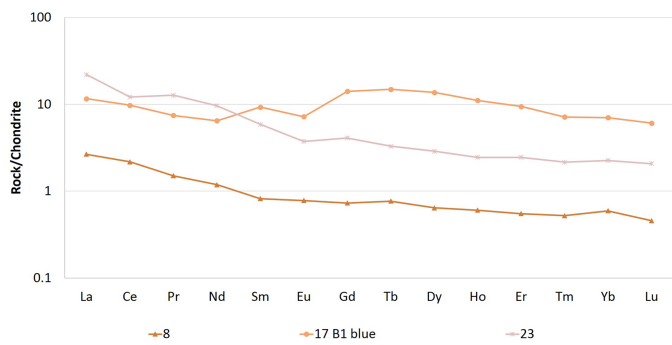
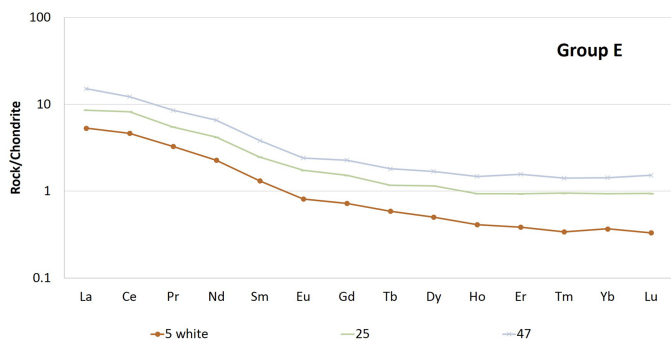
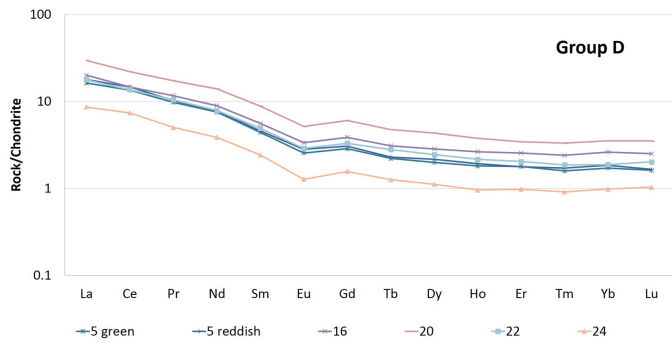
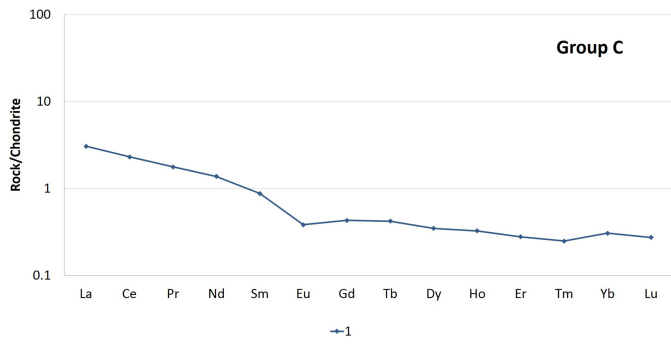
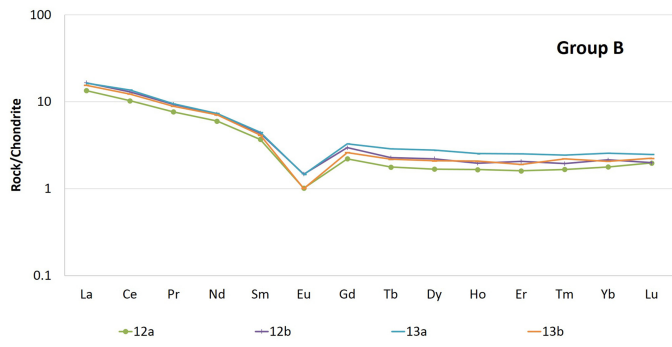
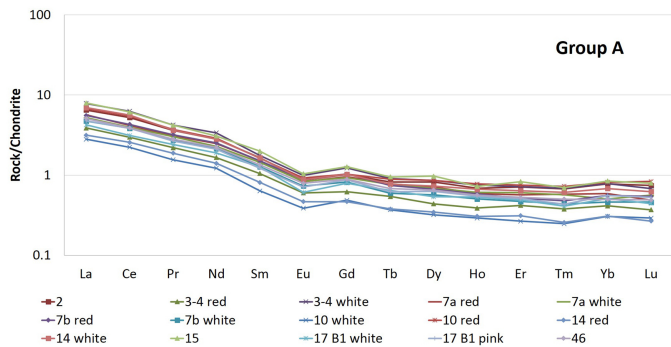


Figure 8